



Influence of transition metal-based activating agent on the properties and catalytic activity of sewage sludge-derived catalysts. Insights on mechanism, DFT calculation and degradation pathways

Pablo Gutiérrez-Sánchez^{a,*}, Silvia Álvarez-Torrellas^a, Marcos Larriba^a, M. Victoria Gil^b, Juan M. Garrido-Zoido^b, Juan García^{a,*}

^a *Catalysis and Separation Processes Group, Chemical Engineering and Materials Department, Faculty of Chemistry, Complutense University, Avda. Complutense s/n, 28040 Madrid, Spain*

^b *Departamento de Química Orgánica e Inorgánica, Facultad de Ciencias and IACYS Unidad de Química Verde y Desarrollo Sostenible, Universidad de Extremadura, E-06006 Badajoz, Spain*

ARTICLE INFO

Keywords:

Activating agents
Catalysts
Density-functional theory
Real wastewater
Sewage sludge

ABSTRACT

Research studies combining the detailed physicochemical properties' analysis, the catalytic activity in different real aqueous matrices, the proposal of degradation mechanisms and the stability of the intermediates/by-products by means of the Density-functional theory (DFT) are scarce. Therefore, this work gives a step forward in the field of circular economy and the removal of emerging pollutants such as the antibiotic ciprofloxacin, covering all the previously aspects mentioned, using four iron and nickel-based catalysts from two different sewage sludge.

Experimental results revealed a significant influence of both the source of the sewage sludge and the activating agent used (iron chloride, nickel chloride and a mixture of both) on the physicochemical properties of the materials and, hence, on their catalytic activity. FTIR studies and chemical composition evidenced that the use of this biomass precursor leads to the generation of a wide variety of functional groups and heteroatoms in the synthesized catalyst structure. Moreover, they showed a combination of Type I-IV isotherms with H3-H4 type hysteresis loops, being mainly mesoporous materials and exhibiting a moderate microporosity except when nickel chloride was used solely as activating agent. The carbonaceous materials reached ciprofloxacin adsorption capacities in the range of 40.4–73.9 mg/g. The use of nickel chloride showed the lowest adsorption contribution and catalytic activity. The bimetallic catalyst (synthesized from a mixture of iron and nickel chloride) showed slightly higher catalytic activity than that found for the iron catalyst, but the metal leaching was also considerably higher. Consequently, the use of iron chloride solely as activating agent seems to be the better alternative, achieving a maximum ciprofloxacin removal around 99.7 % and an iron leaching concentration into the reaction medium of 0.48–0.61 mg/L. The main degradation pathways of ciprofloxacin were proposed according to the detection of LC-MS intermediates and DFT calculation, indicating the most likely areas of attack of reactive species on atoms with a high Fukui index (f^{\ominus}).

1. Introduction

The demand for water is increasing as the world's population grows. Over the years, the fundamental problem limiting our water availability is the pollution of the various aqueous matrices. In this regard, both human and naturally occurring activities contribute to water pollution. The origin of pollution is mainly due to human activities both in urban and industrial areas, hospitals, veterinary clinics, etc [1–4]. Among all

the various pollutants present in water, pharmaceutical residues deserve special attention, organic compounds that are classified as emerging pollutants, mainly due to their persistence in the conventional wastewater treatment plants [5–7].

Pharmaceutical compounds are used every day around the world, either in hospitals for the treatment of human diseases, or in veterinary clinics or farms for the treatment of animal infections. Depending on the chemical characteristics of the pharmaceutical compound, 5 to 90 % are

* Corresponding authors.

E-mail addresses: pgutie03@ucm.es (P. Gutiérrez-Sánchez), jgarcia@ucm.es (J. García).

<https://doi.org/10.1016/j.molliq.2023.121840>

Received 22 December 2022; Received in revised form 12 February 2023; Accepted 11 April 2023

Available online 15 April 2023

0167-7322/© 2023 The Author(s). Published by Elsevier B.V. This is an open access article under the CC BY-NC-ND license (<http://creativecommons.org/licenses/by-nc-nd/4.0/>).

excreted from the body as parent compounds [8–10]. Thus, it can be said that a large amount of pharmaceuticals are consumed in hospitals on a daily basis. In addition, hospitals discharge their wastewater directly into the public sewage system without any pretreatment. It should be noted that several antibiotics are usually present in the natural environment, such as fluoroquinolones, in which ciprofloxacin is included, hold the fourth position in the European market of antibiotics, with a tendency to increase in all countries and been detected in different environmental systems, e.g. soils, sediments, rivers and groundwater, among others [11–14]. Moreover, as antibiotics are highly bioactive compounds, there is high concern about their role in increasing antibiotic resistance among pathogenic bacteria [13]. Thus, numerous studies have been conducted reporting the presence of these pharmaceutical compounds in wastewater treatment plants (WWTPs) as well as into freshwater bodies, where they may be frequently detected at low concentrations [15–18].

On the other hand, activated sludge from a wastewater treatment plant is the main waste from biological treatment [19,20]. It has been estimated that the generation of this waste worldwide (in dry sludge) reached 45 million tons, and its production is expected to continue to grow, predicting a 24 % increase by 2030 and a 51 % increase by 2050 [20,21]. Because these sludges may contain hazardous substances, their adequate treatment is essential [20,22]. In this scenario, it is mandatory to adopt a paradigm shift, in terms of resource consumption by the population to achieve a circular economy. In recent years, several effective sewage sludge treatment technologies have been developed, among which pyrolysis stands out as a promising method, being used to synthesize biochars [23,24]. As these dried sludges contain up to 55–70 % of organic matter, pyrolysis allows reducing carbon by immobilizing it into the biochar [25,26]. Sludge is a biosolid produced worldwide [20,27], and its valorization is a key issue of the circular economy. It is therefore a strategy to change the consumption pattern of the European population towards a circular, climate-neutral economy that minimizes the impact on the environment.

Activated carbons obtained from sewage sludge are generally characterized by their large surface functional groups, moderate-high specific surface area as well as a developed porosity [28–30]. This allows them to be applied in many applications as adsorbents, catalysts or even as soil amendments [30,31]. In recent years, advanced oxidation processes (AOPs) have been widely applied in the treatment of wastewater containing organic pollutants that are difficult to degrade. In these AOP processes, hydroxyl radicals are used to decompose these organic pollutants into smaller molecules or to remove them completely, obtaining CO₂ and H₂O [32,33]. With reference to the advances made in their application to antibiotics removal, several research papers have been reported that allow the removal of these compounds to be studied from a critical point of view [34–37]. In particular, these reports provide information about the degradation of ciprofloxacin from the aqueous environment. For example, Anjali and Shanthakumar published a review article about several treatments, such as UV/H₂O₂, UV/H₂O₂/Fe²⁺, and ozonation that have been used for the removal of ciprofloxacin from wastewater [38]. Some reviews on the application of adsorption process for the removal of this pollutants have also been published [39–41].

However, to our knowledge, there are few studies that report a combination of the behavior of iron and nickel-based catalysts from sewage sludge in the removal of an antibiotic, ciprofloxacin, present in real wastewater, with a Density-functional theory (DFT) study of the degradation mechanism of this compound in two real aqueous matrices.

Therefore, the main objectives of this work are: (1) employ a simple method of reusing sewage sludge as a metal–carbon feedstock to synthesize catalysts by a one-step pyrolysis process, studying the activating agent used, as well as the sludge source, urban or industrial; (2) explore the performance of the system oxidation process, catalytic wet peroxide oxidation (CWPO), using the four synthesized catalysts for the degradation of ciprofloxacin in two real aqueous matrices, and (3) elucidate the degradation mechanisms involved in the CWPO system catalyzed by

the four synthesized catalysts through a Density-functional theory study.

This study is expected to provide a promising utilization strategy to develop a cost-effective sewage sludge-derived catalyst with high efficiency for the degradation of refractory organic pollutants from aqueous medium.

2. Materials and methods

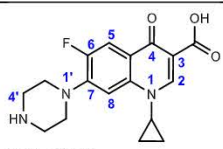
2.1. Chemicals

The synthesis of the catalysts was carried out by using two chemical activating agents, iron(III) chloride hexahydrate and nickel(II) chloride. Hydrochloric acid was added to acidify the aqueous solutions. In addition, acetonitrile and acetic acid were also employed as mobile phases in the analysis of the samples. Ciprofloxacin was selected as a model antibiotic compound to study the catalytic activity of the various catalysts synthesized. Ultrapure water from Veolia PURELAB® Flex Water Purification System was used for the preparation of the aqueous solutions. The structure, suppliers and purity of the aforementioned compounds are listed in Table 1. The sludge applied as biomass precursor of the carbon catalysts was supplied by an urban and an industrial WWTP, specifically this latter from a pharmaceutical industry.

2.2. Synthesis of the catalysts

Firstly, the biomass precursor was dried in an oven at 105 °C. The dried sludge was ground to a fine powder and stored for later use. The ratio used for the chemical activation was 1 g of activating agent per gram of sludge. For the synthesis of the bimetallic catalyst, this ratio was maintained, so each gram of sludge was impregnated with 0.5 g of each of the two activating agents. Then, an aqueous solution of the chemical activating agent was prepared, and the sludge was treated by incipient wetness impregnation method and placed in an ultrasonic bath at 40 °C for 90 min. The latter stage was carried out to favour the access of the activating agent into the sludge pores and to homogenise the mixture. After impregnation, the mixture was left for 12 h at room temperature and then placed in an oven at 105 °C for 24 h to eliminate moisture. The solid obtained was pyrolyzed for 2 h at 800 °C in a vertical quartz reactor, using a nitrogen flow rate of 100 mL/min and a heating rate of 10 °C/min. After grinding, the obtained carbonaceous material was washed with 1 M hydrochloric acid solution for 1 h under magnetic stirring in order to remove the excess metal from the carbon matrix (100 mL HCl 1 M: 1 g carbonaceous material). Finally, it was filtered and washed with ultrapure water until a neutral pH was reached. The catalyst was dried in an oven at 105 °C for 24 h, and crushed and sieved to a particle size lower than 250 µm.

Table 1
Reagents used in the experiments.

Chemical	Structure	Supplier	Purity (wt %)
Ciprofloxacin, CAS n° 85721-33-1		Sigma-Aldrich	≥ 98.0
Ferric chloride hexahydrate, CAS n° 10025-77-1	FeCl ₃ .6H ₂ O	Sigma-Aldrich	>99.0
Nickel dichloride, CAS n° 7718-54-9	NiCl ₂	Sigma-Aldrich	98.0
Hydrochloric acid, CAS n° 7647-01-0	HCl	Fluka	37.0
Acetonitrile, CAS n° 75-05-08	CH ₃ CN	Scharlau	≥ 99.9
Acetic acid, CAS n° 64-19-7	CH ₃ COOH	PanReac	≥ 99.7

2.3. Characterization of raw sludge and catalysts

Macroscopic characterization of sewage sludge was performed using Standard Methods, determining total (TS), fixed (FS) and volatile (VS) solids, and chemical oxygen demand (COD) [42].

The chemical composition of both the biomass precursor and the synthesized catalysts was quantified by X-ray fluorescence spectroscopy (XRF) and elemental analysis (EA), using a PANalytical Axios spectrometer and a LECO CHNS-932 analyser, respectively.

The porosity of the carbonaceous materials was assessed from nitrogen adsorption-desorption isotherms at $-196\text{ }^{\circ}\text{C}$, using a Micromeritics ASAP 2020 analyser. The surface chemistry was evaluated by Fourier-transformed infrared spectrometry, using a Thermo Nicolet Nexus 670 equipment, in a wavelength range of $400\text{--}4000\text{ cm}^{-1}$.

The structural properties were analysed by the X-ray diffraction (XRD) patterns, collected on a Bruker D8 Advance A25 diffractometer, by scanning electron microscopy (SEM) performed in a JEOL JSM 6335F microscope and Transmission electron microscopy (TEM) performed in a JEOL JEM-2100 microscope equipped with a 200 kV LaB6 electron source and with a high-resolution ORUIS SC1000 CCD camera.

Finally, the thermal stability of the materials was tested by thermogravimetric analysis (TGA), that were accomplished in a PerkinElmer STAR 6000 thermobalance. The analyses were conducted using a heating rate of $10\text{ }^{\circ}\text{C}/\text{min}$, a N_2 flow rate of $30\text{ mL}/\text{min}$, and a temperature range of $30\text{--}1000\text{ }^{\circ}\text{C}$.

2.4. Catalytic activity and adsorption contribution

Aqueous solutions of ciprofloxacin were prepared using three aqueous matrices, e.g., ultrapure water, surface water and an urban WWTP effluent. The macroscopic characterization of the two real matrices is detailed in Table 2. The antibiotic concentration was of $50\text{ mg}/\text{L}$, which is in the range reported in the literature for the study of this type of pollutants [17,43–50]. Then, the pH value was modified until reaching the target point at 3.2 by adding 1 M hydrochloric acid.

For the catalytic reactions, 250 mL of ciprofloxacin solution together with the synthesized catalyst ($0.3\text{ g}/\text{L}$) and the required hydrogen peroxide dose ($1.1\text{ mL}/\text{L}$) were introduced into the glass reaction vessel. The operating temperature was of $70\text{ }^{\circ}\text{C}$ and the magnetic stirring was set at 300 rpm . Samples were periodically collected for 180 min and then filtered for further analysis using $0.45\text{ }\mu\text{m}$ PTFE filters. Adsorption tests were performed following the same procedure as previously mentioned, but in the absence of hydrogen peroxide in order to avoid the generation of reaction-initiating hydroxyl radicals.

The concentration of ciprofloxacin was determined by an Agilent HPLC 1260 Infinity II with “diode array” detector, using a Poroshell 120 EC-C18 column ($4.6 \times 150\text{ mm}$; $4\text{ }\mu\text{m}$). A mobile phase consisting of 17.5% acetonitrile and 82.5% acetic acid 75 mM was used, setting a flow rate of $0.85\text{ mL}/\text{min}$, an injection volume of $50\text{ }\mu\text{L}$, a column temperature of $30\text{ }^{\circ}\text{C}$ and a wavelength of 275 nm .

The iron leaching was measured by Inductively Coupled Plasma Optical Emission Spectroscopy (ICP-OES), while the reaction intermediates were identified in a Bruker LC-QTOF-MS Impact II equipment.

Table 2
Macroscopic characterization of real aqueous matrices.

Parameters	Surface water	WWTP effluent
pH	7.3	8.8
Chemical Oxygen Demand (mg/L)	< 15.0	23
Total Organic Carbon (mg/L)	3.2	13.2
Total Carbon (mg/L)	7.4	26.0
Total Nitrogen (mg/L)	0.6	4.8
Total Dissolved Solids (mg/L)	64.0	596.0
Conductivity, at $20\text{ }^{\circ}\text{C}$ ($\mu\text{S}/\text{cm}$)	38.2	484.6

2.5. Computational methods

Gaussian 16 software package was used to perform all computations based on the density functional theory (DFT). Geometric optimization was executed using the hybrid M06-2X method at $6\text{--}311++\text{G}(2\text{df},2\text{pd})$ basis set level, obtaining the corresponding E_{HOMO} (highest occupied molecular orbital) values and positive frequencies in all the possible conformations evaluated, corresponding to minima energy. Here we show, of all these conformations, those that have turned out to be more stable under the conditions of the study, including Natural Bond Orbitals (NBO) analysis [51,52]. The SMD model (universal solvation model based on solute electron density and a continuum model of the solvent defined by the bulk dielectric constant and atomic surface tensions) was used to address the solvent effects of water [53]. GaussView 6.0 software was used to visualize the computed and optimized structures [54], whose coordinates have been included in the Supplementary Material.

The Fukui function has been widely used for the prediction of reactive sites of electrophilic, nucleophilic and radical attack of organic molecules. In this sense, the Fukui function can be defined as [55]:

$$f(r) = \left(\frac{\partial^2 E}{\partial N \cdot \partial v(r)} \right) = \left[\frac{\partial \mu}{\partial v(r)} \right]_N = \left[\frac{\partial \rho(r)}{\partial N} \right]_{v(r)} \quad (1)$$

where $\rho(r)$ is the electron density at point r in space, N is the electron number in the system, and v in the partial derivative is external potential. In the condensed version of the Fukui function, atomic population number is used to represent the electron density distributed around an atom. The condensed Fukui function can be calculated unambiguously for three situations:

$$\begin{aligned} \text{Nucleophilic attack: } f_k^+ &= q_N^k - q_{N+1}^k \\ \text{Electrophilic attack: } f_k^- &= q_{N-1}^k - q_N^k \\ \text{Radical attack: } f_k^0 &= (q_{N-1}^k - q_{N+1}^k)/2 \end{aligned} \quad (2)$$

where k is the number of atoms used in the calculation, N is the number of electrons in the current state, and q^k represents the atomic charge population number of the atom k . In this study, free radical reaction is the most important mechanism, so f_k^0 of ciprofloxacin molecule was employed to study the degradation pathway. The greater the value of f_k^0 , the more vulnerable the site is to free radical attack.

3. Results and Discussion

3.1. Raw sludge characterization

The properties and origin of the biomass precursor have a significant influence on the final characterization of the synthesised carbonaceous materials. Therefore, this work addresses the valorisation of sewage sludge through the synthesis of carbonaceous catalysts, assessing the technical feasibility using sludge from two different sources: an urban and an industrial WWTP. The most relevant characterization parameters are summarized in Table 3.

Sewage sludge typically has a high organic matter content, which makes it potentially suitable for its use in the synthesis of carbonaceous materials [30]. COD and vS values indirectly indicate the organic matter content of the sewage sludge, being considerably higher for industrial sludge (COD = $34.8\text{ g}/\text{L}$; vS = $29.3\text{ g}/\text{L}$) compared to the urban one (COD = $8.4\text{ g}/\text{L}$; vS = $6.5\text{ g}/\text{L}$). The TS value of the industrial sludge is about 4 times larger than the urban sludge (36.6 vs $8.8\text{ g}/\text{L}$), indicating a higher water content in the sludge supplied by the urban WWTP. However, both sludges presented an approximately equal percentage of volatile matter over total solids content, being within the range $74\text{--}80\%$. In this regard, high values of volatile matter will not only promote the generation of porosity but also increase the efficiency of the carbon synthesis. In the literature, a volatile matter content higher than 70% is usually recommended, so the two sludges used in this study seem to be

Table 3
Characterization of the raw sludges.

Parameters	Industrial	Urban
<i>Macroscopic characterization (g/L)</i>		
Chemical Oxygen Demand	34.8	8.4
Density	1000.6	955.9
Total Solids	36.6	8.8
Volatile Solids	29.3 (80 %)	6.5 (74 %)
Fixed Solids	7.3 (20 %)	2.3 (26 %)
<i>Chemical composition of the dried sludge (wt.%)</i>		
C	42.4	37.9
O	14.6	18.9
H	5.8	5.6
N	3.7	6.1
Fe	0.7	11.6
Ni	0.4	0.02
Ca	11.7	3.0
S	0.7	0.7
Si	0.73	2.63
Cl	3.5	0.6
Na	2.3	–
P	1.9	4.8
K	1.4	1.9
Al	0.6	1.0

suitable biomass precursors [56]. Finally, the FS content of both urban and industrial sludge is related to the ash content, and is within the values found in the literature for this type of biomass precursor [30,57,58].

The chemical composition of both sludges showed a predominant contribution of carbon (38–42 %) and oxygen (15–19 %), which, together with the hydrogen content, are within the range reported by other authors for this kind of biomass source [30,58–61]. According to the literature, the carbon content required to achieve acceptable carbon yields has to be in the range of 40–90 %, so the industrial sludge would be within it and the urban sludge would be very close to it. Therefore, it seems that both sludges could be potential biomass precursors for the synthesis of carbonaceous materials [62,63].

Sulphur and nitrogen contents in raw sludges were found relatively low. Thus, the emissions of these oxides during the pyrolysis process could be considered as negligible, minimizing the impact of these harmful gases on the environment [56].

The predominant metal concentration found in the urban sludge was iron (11.6 %), while in the industrial sludge it was calcium (11.7 %). A high concentration of these metals in various types of sludge has been reported in the literature [30,64–66]. Other minor elements were potassium, phosphorus, sodium, chlorine, sodium, or silicon. The sludge chemical composition is quite heterogeneous and variable, and its properties can change significantly depending on the sludge source, day or location [66].

3.2. Catalyst characterization

3.2.1. Chemical composition

As can be seen in Table 4, the source of the biomass precursor seems to have a significant influence on the final catalyst composition when the same synthesis conditions and activation agent were used. That is, although the initial carbon content for both precursors was approximately the same, the pyrolysis process generated very different final compositions. While the industrial sludge provided catalysts with a carbon content of more than 70 wt%, the urban sludge only reached to 23 wt%. Therefore, the carbon content of Urban-Fe was lower than that of the biomass precursor, while the carbon content of the industrial-sludge catalyst was higher. This trend evidenced a difference in the pyrolysis mechanisms depending on the composition of the sewage sludge used as precursor, as reported in other studies [30,64].

Also, noteworthy is the high oxygen contribution of the Urban-Fe catalyst (28.3 wt%), compared to the Industrial-Fe sample (8.5 wt%).

Table 4
Influence of the sludge source and activating agent on the final composition of the catalysts.

Parameters	Urban-Fe (wt.%)	Industrial-Fe (wt.%)	Industrial-Ni (wt.%)	Industrial-FeNi (wt.%)
C	23.1	70.9	50.5	52.9
O	28.3	8.5	13.6	14.4
H	2.8	1.8	1.6	1.5
N	4.5	3.8	2.1	2.1
Fe	9.3	5.1	0.1	8.7
Ni	0.08	0.2	26.8	15.8
Ca	0.7	0.6	0.6	0.4
S	0.5	1.2	1.0	0.9
Si	14.9	3.4	0.6	1.0
Cl	4.8	2.4	0.8	0.4
Na	–	–	–	–
P	1.4	0.9	1.7	1.5
K	3.0	0.02	0.01	0.01
Al	3.2	1.0	0.3	0.3

This could be attributed to the high iron content present in the urban sludge, which could favour its combination with the oxygen present in the sample to generate metal oxides, increasing the oxygen content in the carbon material [64]. Moreover, the iron content obtained with the urban sludge precursor was slightly lower than twice that obtained with the industrial sludge. The higher attachment of this metal to the carbonaceous matrix could have been favoured by the high iron content of the raw urban sludge. Silicon was also one of the major elements in the Urban-Fe catalyst (14.9 wt%).

Regarding the influence of the activating agent, the composition of three catalysts obtained from the same biomass precursor, i.e. industrial sludge, was compared. The activating agents applied were iron and nickel salts, and a mixture of both. As can be seen in Table 4, it was observed a considerably higher carbon content for the catalyst synthesized with iron chloride (Industrial-Fe) compared to that obtained using nickel chloride (Industrial-Ni). The bimetallic catalyst (Industrial-FeNi) showed an intermediate value to those obtained for the previous ones, although much closer to the Industrial-Ni catalyst. The oxygen contribution was considerably higher for the two Ni-based catalysts, either pure or as a mixture with the iron salt (13.6 and 14.4 wt%). That is, while the industrial-Fe catalyst reduced the oxygen content to about half of that present in the raw sludge (14.6 wt%), the Ni and bimetallic catalysts showed a negligible variation. The type of chemical activation agent did not seem to have a significant influence on the hydrogen, sulphur or potassium content. However, the nickel salt used in the Industrial-Ni and Industrial-FeNi catalysts led to a slight decrease of the chlorine, nitrogen and silicon content in the final composition of the carbon materials. The potassium content seemed to show the opposite trend, rising as the amount of nickel chloride impregnated in the catalyst increased.

A marked difference in the amount of active phase attached to the carbonaceous matrix was also observed for the Industrial-Fe and Industrial-Ni catalysts. While a 26.8 wt% of nickel was found in the Ni-based catalyst, the Industrial-Fe material only achieved a 5.1 wt% of iron. That is, the activating agent seemed to show a significant influence on the attachment of the active phase, showing a favourable trend in the case of the nickel salt. However, despite having a higher metal content, the Industrial-Ni catalyst may have a lower catalytic activity than the Industrial-Fe material, as will be discussed in the following sections.

Furthermore, it would be expected that, by using a lower relative amount of iron and nickel chloride in the synthesis of the Industrial-FeNi catalyst (1 g dried sludge: 0.5 g iron salt: 0.5 g nickel salt), the content of these metals in the final sample would be between the values for the catalysts obtained from a single metal salt, i.e. Industrial-Fe (1 g dried sludge: 1 g iron salt) and Industrial-Ni (1 g dried sludge: 1 g nickel salt). However, the bimetallic catalyst showed a higher iron concentration than the Industrial-Fe catalyst, while the nickel content was lower than

that found in the Industrial-Ni catalyst. It seems that the use of a bimetallic solution in the incipient wetness impregnation method favoured the iron attachment on the carbonaceous matrix, while nickel attachment was reduced. It should also be noted that the rinsing step during the catalyst synthesis mostly removed the calcium in the industrial sludge-based catalysts, obtaining values lower than 0.6 wt%.

Pyrolysis processes allowed to obtain carbonaceous materials from diverse biomass sources. During this stage, smaller organic molecules condense into conjugated aromatic rings, and organic nitrogen and metals can also be conjugated into the carbonaceous structure. This resulted in metal loading sites, oxygen functionalities, defective edges and nitrogen doping [67]. Compared to other biomass precursors, the use of sewage sludge favoured the generation of functional groups in the carbonaceous materials [64]. For this reason, the chemical composition of the catalysts synthesized with the two sludges and the different chemical activating agents showed carbon content values lower than those found for commercial activated carbons (around 90 %) [58].

3.2.2. Porosity

The porosity of carbonaceous materials is one of the most important properties, since it will determine the feasibility of the materials for applications such as catalysis and/or adsorption. This information has been obtained from the nitrogen adsorption-desorption isotherms at

−196 °C.

The behaviour of the synthesized catalysts when exposed to a physisorption process under a nitrogen atmosphere, as shown in Fig. 1a, seems to suggest a combination of Type I-IV isotherms. This pattern has been previously reported in the literature for carbonaceous materials obtained from sewage sludge, and it is characteristic of mesoporous solids, with a moderate contribution of microporosity [30,60,65]. In addition, all four materials showed a hysteresis loop at P/P^0 values close to 0.4, which is often found in micro-mesoporous carbons [68]. This is, H3-H4 Type hysteresis loops, as found for the synthesized catalysts, indicated the occurrence of narrow crack pores and slit-shaped pores in the carbon structure [65,69,70]. A steep nitrogen uptake was observed at low relative pressures, which is related to the microporosity contribution in the analysed samples [68,71].

In addition, the desorption branches showed a step-down at P/P^0 values close to 0.5, which might indicate cavitation induced by the evaporation of the condensed liquid in larger mesopores (capillary condensation effect) [72]. This behaviour seems not to depend on the biomass source, i.e. Urban-Fe and Industrial-Fe catalysts exhibited a similar shape. However, the catalysts in which nickel salt was used as activating agent (Industrial-Ni and Industrial-FeNi) this phenomenon appeared to be increased, showing a sharper step down.

As has been reported in the literature, the BET (Brunauer-Emmett-

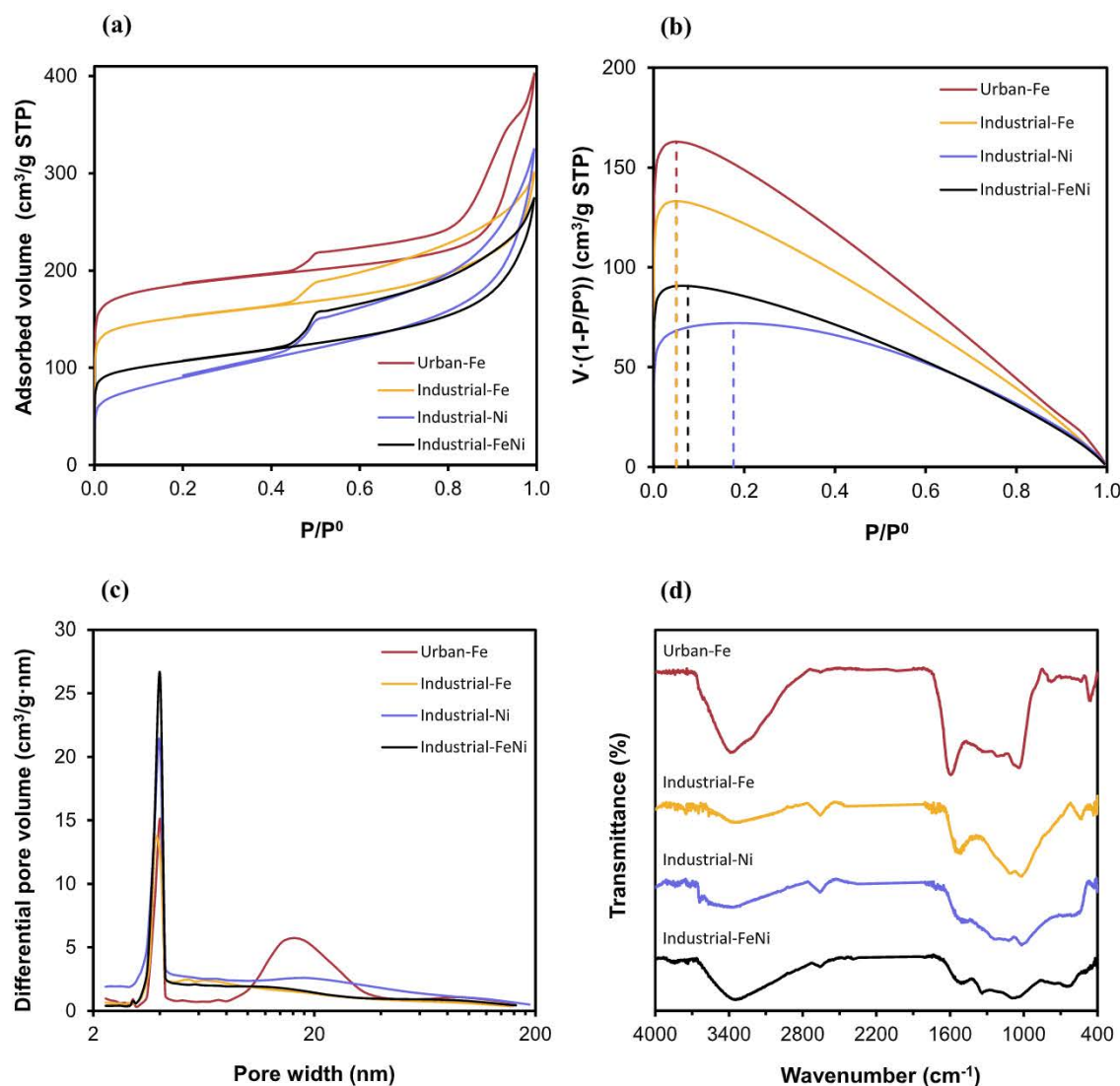


Fig. 1. N_2 adsorption-desorption isotherms (a), BET calculation criteria (b), Pore size distribution calculated with BJH method (c), and FTIR spectra (d) of the synthesized catalysts with different activating agents and sludge source.

Teller) method can be applied to Type IV and II isotherms, where the linearity range of the BET plot is usually found in the relative pressure range of 0.05–0.3. However, the presence of micropores hinders the application of this method, as it may be not possible to separate the micropore filling and monolayer-multilayer adsorption processes, and the standard range of relative pressures is no longer valid. In this case, the linear range of BET plot may be narrow and difficult to locate. To address this issue, Rouquerol et al. proposed a procedure to determine the correct relative pressure range and avoid any subjectivity during the evaluation of the BET monolayer capacity [68,72–74]. Since the catalysts synthesized have a considerable microporosity, these criteria have been used to determine the BET surface area.

The upper relative pressure limit of the BET range, which corresponded to the absolute maximum shown in dashed lines in Fig. 1b, reached values of 0.05 for Urban-Fe and Industrial-Fe catalysts, 0.18 for Industrial-Ni and 0.08 for Industrial-FeNi. Therefore, it seems that a high microporosity in the material increased the narrowing of the applicable relative pressure range. Table 5 shows the calculated values of the apparent BET surface area by applying the previously mentioned procedure for micro-mesoporous materials. The apparent S_{BET} values decreased in the following order: Urban-Fe > Industrial-Fe > Industrial-FeNi > Industrial-Ni. A high apparent BET monolayer capacity was found when urban sludge was used as biomass precursor and when increasing the amount of iron chloride used as chemical activating agent. The resulting BET values are within the range reported in the literature for other carbonaceous materials obtained from sewage sludge by chemical activation with iron chloride ($S_{\text{BET}} = 468 \text{ m}^2/\text{g}$) and zinc chloride ($S_{\text{BET}} = 266\text{--}558 \text{ m}^2/\text{g}$) [30,60]. Moreover, the chemical activation agents proposed in this study exhibited apparent S_{BET} higher than those obtained by other authors for chemical activation agents such as iron nitrate ($S_{\text{BET}} = 240 \text{ m}^2/\text{g}$), iron sulphate ($S_{\text{BET}} = 233 \text{ m}^2/\text{g}$), or (ortho)-phosphoric acid ($S_{\text{BET}} = 230\text{--}296 \text{ m}^2/\text{g}$) [30,60,71]. According to Álvarez et al., the physical activation of sewage sludge, without any pre-treatment of the raw sludge, allowed to obtain carbonaceous materials with an apparent S_{BET} of $43 \text{ m}^2/\text{g}$, values considerably lower than those obtained by chemical activation following the procedure described in this work [75].

On the other hand, nitrogen adsorption–desorption isotherms provided other textural parameters, such as the contribution of microporosity (V_{Micro}) and mesoporosity (V_{Meso}) to the total pore volume (V_{Total}), as well as the average pore width. This information is summarized in Table 5.

The total pore volume, i.e. the maximum amount of N_2 uptake at a relative pressure close to 1.0 decreased in the following order: Urban-Fe > Industrial-Ni > Industrial-Fe > Industrial-FeNi. However, the relative micropore volume showed a different trend: Industrial-Fe > Urban-Fe > Industrial-FeNi > Industrial-Ni. Therefore, while the iron chloride used as activating agent seems to show a slight decrease in the total pore volume, the development of microporosity was considerably favoured. Furthermore, the use of a mixture of iron and nickel chloride as chemical activating agent resulted in a catalyst whose V_{Total} was lower than those

Table 5
Porosity-related properties of the synthesized catalysts.

Parameters	Urban-Fe	Industrial-Fe	Industrial-Ni	Industrial-FeNi
S_{BET} (m^2/g)	713	582	319	397
V_{Micro} (cm^3/g) ^a	0.219	0.173	0.030	0.100
V_{Meso} (cm^3/g) ^c	0.404	0.293	0.472	0.325
V_{Total} (cm^3/g) ^b	0.623	0.466	0.502	0.425
$V_{\text{Micro}}/V_{\text{Total}}$ (%)	35.1	37.1	6.0	23.6
Average pore width (nm)	10.4	7.2	7.1	6.8

^a Calculated by Dubinin–Radushkevich method.

^b Volume of pores at $P/P^0 = 0.99$.

^c Calculated from V_{Micro} and V_{Total} .

values of catalysts synthesized with a single activating agent (Industrial-Fe and Industrial-Ni), but the relative microporosity was found to be in between these two.

It should be noted that the heterogeneity in the composition depending on the sludge source appeared to have a significant influence on the final porosity of the synthesized carbonaceous materials. In this regard, while the use of urban sludge (Urban-Fe) showed a considerably high total pore volume, the relative contribution of microporosity was slightly lower than that obtained for the Industrial-Fe catalyst. The development of a higher total porosity with the urban sludge could be due to the high iron content found in the dried raw sludge (11.6 wt%). This means that the chemical activation during the catalyst synthesis could have been due to both the contribution of the impregnated iron chloride and the iron content of the raw sludge. The increase in relative micropore volume when industrial sludge was used could be attributed to the high calcium content present in the raw sludge (see Table 3), which was removed during the catalyst rinsing (see Table 4), unblocking the pores that were occupied in the carbonaceous matrix.

According to the literature, the different pore structure generated during the pyrolysis process for the synthesis of carbonaceous materials from sewage sludge is related to the varying inorganic content depending on the source. However, most authors have reported a simultaneous formation of mesopores and micropores in both physical and chemical activation [75].

Pore size distribution is one of the established criteria for the selection of carbonaceous materials in applications such as adsorption, determining the fraction of the volume accessible to molecules of a particular shape or size [76]. The pore size distribution of the catalysts (Fig. 1c) highlights the micro-mesoporous nature of the materials, reaching a maximum around 4 nm for all catalysts. The Urban-Fe catalyst also showed another relative maximum around 16 nm. As shown in Table 5, the chemical activation of sewage sludge with iron and nickel chloride allowed the synthesis of predominantly mesoporous carbonaceous materials, with average pore width values ranging from 6.8 to 10.4 nm. These values justify the loop hysteresis found in the N_2 adsorption–desorption isotherms (see Fig. 1a), since this phenomenon occurs when the pore width exceeds a critical value, which for nitrogen at $-196 \text{ }^\circ\text{C}$ is 4 nm [72].

Iron and nickel salts used as chemical activating agents have been effective in the synthesis of carbonaceous materials, exhibiting high porosity and surface area. These compounds promoted the degradation of the biomass precursor used as carbon source, generating a dehydration of the raw material that resulted in the carbonisation and aromatisation of the carbon skeleton and developing the porous structure [76]. As a result, biochars of a micro-mesoporous nature were obtained, which is in agreement to the data reported by other authors [65].

3.2.3. Surface chemistry

The surface functional moieties of the catalysts are generally assessed from the Fourier-transformed infrared (FTIR) spectra, shown in Fig. 1d.

As can be observed, all catalysts showed a broad band located between 3700 and 2800 cm^{-1} , which could be related to both the presence of O–H bonds on the catalyst surface and the moisture adsorbed by the materials [30,77]. The intensity of this band decreased in the following order: Urban-Fe > Industrial-FeNi > Industrial-Ni > Industrial-Fe, being in agreement with the oxygen content of the materials, shown in Table 4. This band could also be attributed to the N–H stretching vibrations related to amides and amines from the proteins found in the sewage sludge [75]. However, the low nitrogen content compared to oxygen in the final catalysts seemed to suggest a higher contribution of O–H bonds of the synthesized materials.

The synthesized materials also showed a band around 2650 cm^{-1} , which could be attributed to aliphatic C–H stretching vibrations [30].

All four catalysts showed a peak at a wavelength around 1600 cm^{-1} , which could be related to C=O and/or C=C bonds of carbonyl groups

(belonging to functional groups such as ketones, quinones, keto-esters, diketones and ketoenols) and aromatic rings, respectively [78–80]. This peak seemed to be extremely dependent on the biomass source used in the synthesis, reaching considerably higher values for Urban-Fe material compared to Industrial-Fe. This fact could be favoured by the high oxygen content of the Urban-Fe catalyst (see Table 4), being involved in the formation of carbonyl bonds.

The band found between 1000 and 1200 cm^{-1} could be explained by the C—O stretching from alcohols, phenols, acids, ethers or ester functional groups [78,80,81]. In addition, the absorption peaks located from 900 to 1200 cm^{-1} might be related to Si—O—Si and Si—O—C bonds, which could explain the high intensity of this band for the Urban-Fe catalyst due to its higher silicon content (see Table 4) [75].

Finally, the band located in the wavelength range 400–800 cm^{-1} could indicate the out-of-plane bending vibration of O—H bonds or the stretching vibration of C—H (benzene derivatives) bonds. The presence of these aromatic C—H groups would suggest the surface aromatization of these carbonaceous catalysts [30,82].

3.2.4. Structural properties

In order to characterize the crystalline phases present in the sewage sludge-derived catalysts, XRD studies were accomplished. The XRD patterns obtained are shown in Fig. 2. Thus, XRD patterns for the catalysts containing only iron, named as Urban-Fe and Industrial-Fe, exhibited three main wide peaks, characteristic of poor crystalline solids, located at 2θ values of 26° and 43°, which correspond to graphite phase (ICDD PDF File 001–0646) and were assigned to (002), (100)–(101) planes. The XRD graphs of these materials did not show peaks which could origin from iron in metallic form [83]. Moreover, it should be highlighted that if the particle size of iron is very small, it could not be observed in XRD patterns. On the other hand, the XRD patterns of the Ni-based catalysts (Industrial-Ni and Industrial-FeNi) showed three large reflection signals (as illustrated in Fig. 2) at 44.6° (111) 51.9° (200) and 76.4° (220), typical of metallic nickel with a FCC structure [84]. These peaks are more intense than those observed in the XRD patterns of iron-based catalysts, since the percentage of Ni used in the synthesis was much higher (Table 4).

The SEM micrographs of the synthesized catalysts are shown in Fig. 3a–d. All the micrographs revealed a morphology characteristic of porous materials, where inner porosity has been developed through a thermal treatment. In Fig. 3a, the largely isolated cylindrical units have

walls formed by layers of thin films. In Fig. 3b, these units seen in Fig. 3a have coalesced at the walls into a singular solid matrix interspersed with pores. The bonding of the walls and the melting of the wall lamellae suggested a deep transformation at molecular level in the sewage sludge during pyrolysis. Generally, all the carbon samples showed a great heterogeneity.

3.2.5. Thermal stability

Thermal stability is a key requirement for the catalysts, and it will limit both the operating conditions under which they can be used and their suitability for thermal regeneration after their application. The thermogravimetric analysis of the four synthesized catalysts are shown in Fig. 4.

Firstly, there is a weight loss of the samples around 100 °C, which could be related to the water adsorbed on the carbonaceous materials. According to the results obtained, both the source of the sludge and the activating agent seemed to have an influence on the sample moisture. That is, while Industrial-Fe material presented moisture values close to 7 %, Urban-Fe reached to 12.2 %. In addition, Industrial-Ni catalyst showed a moisture content close to 5.1 %, which is lower than that observed for Industrial-Fe. However, the use of a mixture of activating agents consisting of iron and nickel chloride seemed to favour water adsorption, reaching values close to 7.9 % for the Industrial-FeNi catalyst. Therefore, the moisture content of the synthesized catalysts decreased in the following order: Urban-Fe > Industrial-FeNi > Industrial-Fe > Industrial-Ni.

All samples showed a slightly decreasing trend in weight at temperatures above 100 °C, which could be associated with the decomposition of compounds that did not have time to degrade during the pyrolysis process in the catalyst synthesis. Moreover, at temperatures close to the pyrolysis temperature, i.e. between 700 and 900 °C, a more steep weight variation was observed, which could be mainly due to the removal of compounds that require a higher pyrolysis temperature or time than the one used in the synthesis. It should be noted that the Industrial-Fe catalyst was the material with the lowest weight variation, i.e. the one with the highest thermal stability.

3.3. Catalytic Wet Peroxide Oxidation of Ciprofloxacin

3.3.1. Adsorption tests

Carbonaceous materials derived from pyrolytic processes using biomass precursors generally exhibit adsorptive properties as a consequence of the porosity generated during their synthesis. In this study, the porous nature of the four synthesized catalysts has been described by their characterization in the previous section. In other words, the information obtained from the N_2 adsorption–desorption isotherms, together with the surface chemistry of the materials, will lead to different kinetics and adsorption capacities depending on the activating agent and the source of the sludge used in the synthesis of the carbon materials.

Therefore, to evaluate the effectiveness of the catalysts in the heterogeneous reaction systems, adsorption blanks are required to assess the contribution of adsorption to the pollutant removal process. This information can be seen in Fig. 5.

With regard to the influence of the source of biomass precursor, the catalyst synthesized from industrial sludge (Fig. 5b) appeared to exhibit considerably slower adsorption kinetics compared to that shown for the material obtained from urban sludge (Fig. 5a). That is, while the Urban-Fe catalyst required times longer than 45 min to reach the equilibrium, an equilibrium time higher than 120 min was needed for the Industrial-Fe catalyst.

On the other hand, the type of activating agent used for the catalyst synthesis also seemed to show some influence on the adsorption kinetics. Zinc chloride allowed obtaining carbons with faster adsorption kinetics than those shown with iron chloride. Specifically, Industrial-Ni catalyst (Fig. 5c) required times longer than 60 min to reach the equilibrium,

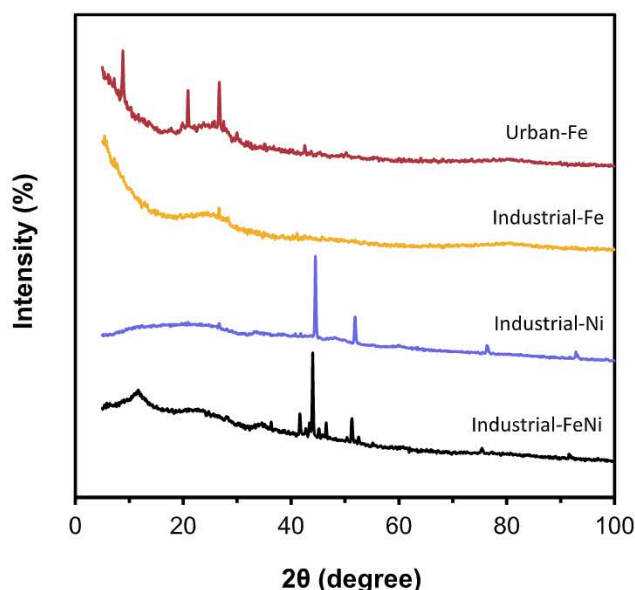


Fig. 2. XRD patterns of the catalysts synthesized with different activating agents and sludge source.

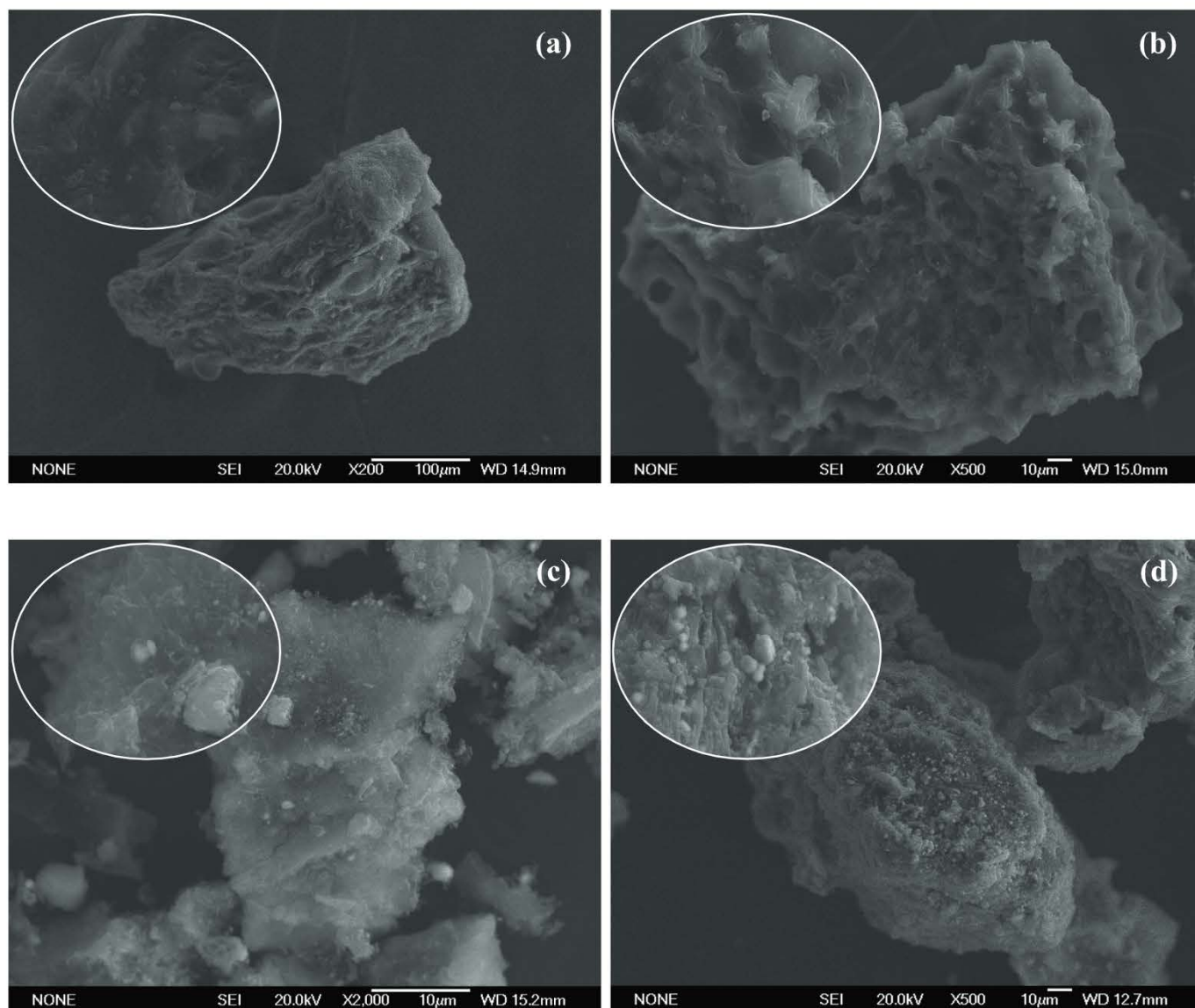


Fig. 3. SEM micrographs of the catalysts synthesized with different activating agents and sludge source: Urban-Fe (a), Industrial-Fe (b), Industrial-Ni (c), Industrial-FeNi (d).

compared to the equilibrium time shown by the previously mentioned Industrial-Fe material. Furthermore, it should be noted that the use of a mixture of activating agents consisting of iron and nickel chloride for the synthesis of the bimetallic Industrial-FeNi catalyst (Fig. 5d) presented similar kinetics to that obtained for the Industrial-Fe catalyst. Therefore, the iron chloride predominantly seemed to determine the kinetics of the bimetallic catalyst, making the time required to reach the equilibrium the same as for the Industrial-Fe, i.e. 120 min.

The adsorption capacity at equilibrium time, defined by Equation 3, is one of the most commonly used parameters to compare the adsorption contribution of different materials.

$$q_e = \frac{C_{\text{Ciprofloxacin},0} - C_{\text{Ciprofloxacin},e}}{C_{\text{Catalyst}}} \quad (3)$$

where q_e (mg/g) is the adsorption capacity at equilibrium time; $C_{\text{Ciprofloxacin},0}$ (mg/L) is the initial ciprofloxacin concentration, i.e. 50 mg/L; $C_{\text{Ciprofloxacin},e}$ (mg/L) is the concentration of ciprofloxacin when equilibrium was reached, assuming that the equilibrium time corresponded to the last sample taken at 180 min; and C_{Catalyst} (g/L) is the catalyst dose used, i.e. 0.3 g/L.

As observed, both the biomass source and the activating agent seemed to have an influence on the ciprofloxacin concentration in the aqueous phase at equilibrium time, assuming that equilibrium has been reached at approximately 180 min. In this regard, the equilibrium concentration values were of 30.1, 27.8, 37.9, and 30.2 mg/L for Urban-Fe, Industrial-Fe, Industrial-Ni, and Industrial-FeNi catalysts, respectively. Therefore, the adsorption capacity values of the synthesized materials were 66.3, 73.9, 40.4, and 66.0 mg/g, respectively, in the order previously indicated. The adsorption capacity range of the synthesized materials is in accordance with the one reported in the literature for other biomass-based materials for the removal of ciprofloxacin [85–88] and other emerging contaminants [30,60].

As previously discussed, the sludge source and the activating agent have an influence on the kinetics and adsorption capacity of the catalysts. While the adsorption rate decreased in the following order: Urban-Fe > Industrial-Ni > Industrial-Fe = Industrial-FeNi; the adsorption capacity did so as follows: Industrial-Fe > Urban-Fe \approx Industrial-FeNi > Industrial-Ni.

Finally, the study of the aqueous matrix effect on the adsorption process evidenced a relatively small effect on the four materials considered. As can be seen, although the kinetics seemed to maintain a

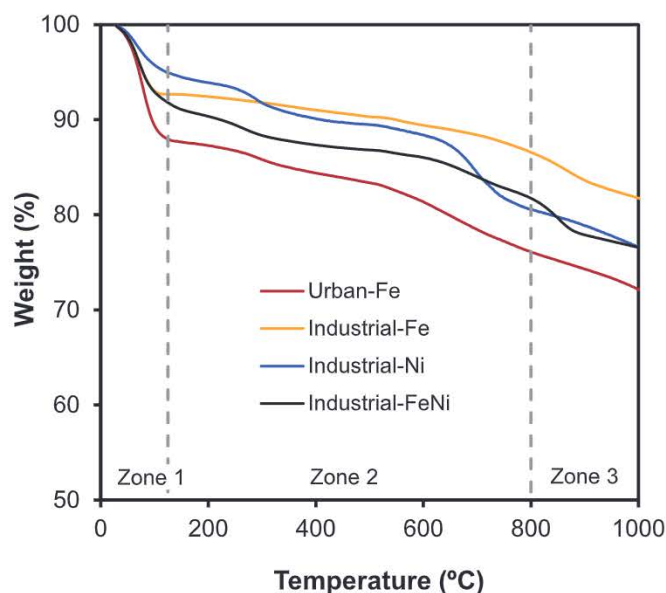


Fig. 4. Thermogravimetric profiles of the synthesized catalysts with different activating agents and sludge source.

similar trend regardless of the matrix, the ciprofloxacin concentrations in the aqueous phase increased in the following order: ultrapure water < surface water < WWTP water. The higher removal of the antibiotic in ultrapure water compared to the real aqueous matrices could be due to the presence of other organic and inorganic compounds competing for the active sites of the solid for the adsorption of ciprofloxacin. Therefore, it seemed that an increase of organic and inorganic matter in the real matrix led to a lower adsorption capacity, i.e. a higher ciprofloxacin equilibrium concentration in the aqueous phase. This could explain the lower ciprofloxacin concentration when using surface water compared to that found in WWTP effluent, since macroscopic parameters, such as the chemical oxygen demand, total organic carbon, total dissolved solids, among others, were considerably higher for the latter (see Table 2).

3.3.2. Catalytic activity

The properties and catalytic activity of the catalysts will determine the removal rate of ciprofloxacin, as well as the formation of different reaction intermediates and by-products. Thus, the evolution of the relative concentration of the tested antibiotic in the reaction tests, using the four synthesized catalysts and the three aqueous matrices, has been illustrated in Fig. 6.

As can be seen, the degradation kinetics of ciprofloxacin using the Urban-Fe catalyst, Fig. 6a, was considerably slower than that shown for the Industrial-Fe, Fig. 6b. That is, while the former needed times longer than 180 min to reach a ciprofloxacin removal of around 98 %, the Industrial-Fe catalyst did so before 30 min. Moreover, the reaction profile for Urban-Fe catalyst before 15 min was identical to that shown in the adsorption profile (see Fig. 5), suggesting that the major contribution in the ciprofloxacin removal up to that time is from adsorption. This could be due to the formation of a minimum concentration of hydroxyl radicals in the oxidation process that initiates the reaction. However, this time seems to be considerably reduced for the Industrial-Fe catalyst, with the adsorption and reaction profiles coinciding only up to the first 5 min.

It should also be noted that the iron content of the Industrial-Fe catalyst (5.1 wt%) was considerably lower than that of the Urban-Fe material (9.3 wt%). However, the catalytic activity showed the opposite trend. This behaviour could indicate a higher dispersion and accessibility of the active phase on the catalyst surface, which could lead to a higher metal leaching. HR-TEM images of the particle size

distribution and metallic dispersion of the iron and nickel particles of the catalysts are presented in Fig. S1, the histograms of metals particle size distributions are shown in Fig. S2, supporting information. The average particle size of the iron or nickel particles of the catalysts was obtained by counting using ImageJ software. The results indicated a mean particle size distribution of 46 ± 17.94 , 67 ± 23.54 , 32 ± 9.63 and 34 ± 16.33 nm, for Urban-Fe, Industrial-Fe, Industrial-Ni and Industrial FeNi catalysts, respectively. In addition, by TEM images, the better dispersion of iron metal on the surface of Industrial-Fe catalyst, with respect to Urban-Fe catalyst, is confirmed. Indeed, the values of the iron leached concentration into the reaction medium were slightly higher for the Industrial-Fe catalyst compared to those observed for the Urban-Fe catalyst. Specifically, the iron concentrations in the reaction medium at near 98 % ciprofloxacin removal were of 0.48 mg/L (at 180 min reaction time) and 0.61 mg/L (at 30 min reaction time) for the Urban-Fe and Industrial-Fe catalysts, respectively. Therefore, the origin of the sludge has a considerable influence on the catalytic activity of the carbonaceous catalyst.

Concerning the influence of the activating agent on the ciprofloxacin removal kinetics, nickel appeared to have a significantly lower catalytic activity than iron. That is, while the Industrial-Fe catalyst achieved a maximum ciprofloxacin removal of 99.7 %, the Industrial-Ni catalyst reached only 32.5 % (Fig. 6c). It is also noteworthy that the concentration of nickel in the Industrial-Ni material (26.8 wt%) was considerably higher than that of iron in the Industrial-Fe catalyst (5.1 wt%), again highlighting the low catalytic activity of nickel in the generation of hydroxyl radicals for the CWPO process.

As previously mentioned, the presence of iron in the catalyst seemed to considerably favour the kinetics of the process. However, the bimetallic Industrial-FeNi catalyst (Fig. 6d) showed faster removal kinetics than the Industrial-Fe catalyst. This behaviour could be due to the high iron (8.7 wt%) and nickel (15.8 wt%) content of the former, although due to the low nickel catalytic activity it is likely to have been caused mainly by iron. That is, while the Industrial-FeNi catalyst required 15 min to remove the antibiotic almost completely, the Industrial-Fe catalyst required 15 min longer. In addition, due to the higher metal content in the Industrial-FeNi catalyst, the leaching into the reaction medium also increased. Specifically, the concentration of iron and nickel in the reaction medium when reaching around 98 % ciprofloxacin removal was 2.0 and 11.4 mg/L, respectively. Therefore, although the reaction kinetics was slightly favoured in the bimetallic catalyst due to the higher iron content, the leaching of metals into the reaction medium was higher, and the Industrial-Fe catalyst could be considered as the optimum material. In other words, the activating agent has a crucial influence on the catalytic activity of the synthesized carbonaceous materials, being preferable the use of iron chloride over nickel chloride.

The initial reaction rates were calculated by numerical derivation from the concentration profile versus time and collected in Table 6. These values evidenced the kinetic behaviour previously discussed. That is, the reaction rate depends on both the origin of the sludge and the active agent, decreasing as follows: Industrial-FeNi > Industrial-Fe > Urban-Fe > Industrial-Ni. Furthermore, the reaction kinetics and the catalytic activity seem to depend on the aqueous matrix and, as observed in the adsorption tests, decrease in the following order: ultrapure water > surface water > WWTP water. This effect could be related to the occurrence of other pollutants in the real aqueous matrices that would compete with ciprofloxacin during the catalytic wet peroxide oxidation. Therefore, as shown in Table 2, the higher pollutant concentration in WWTP water compared to surface water would disfavour the ciprofloxacin reaction rate.

3.3.3. Mechanism and pathways of CWPO degradation of ciprofloxacin. DFT study

The possible mechanism of ciprofloxacin removal on the catalyst (urban or industrial)/hydrogen peroxide could be as follows: When hydrogen peroxide is present, the iron or nickel ions on the catalyst

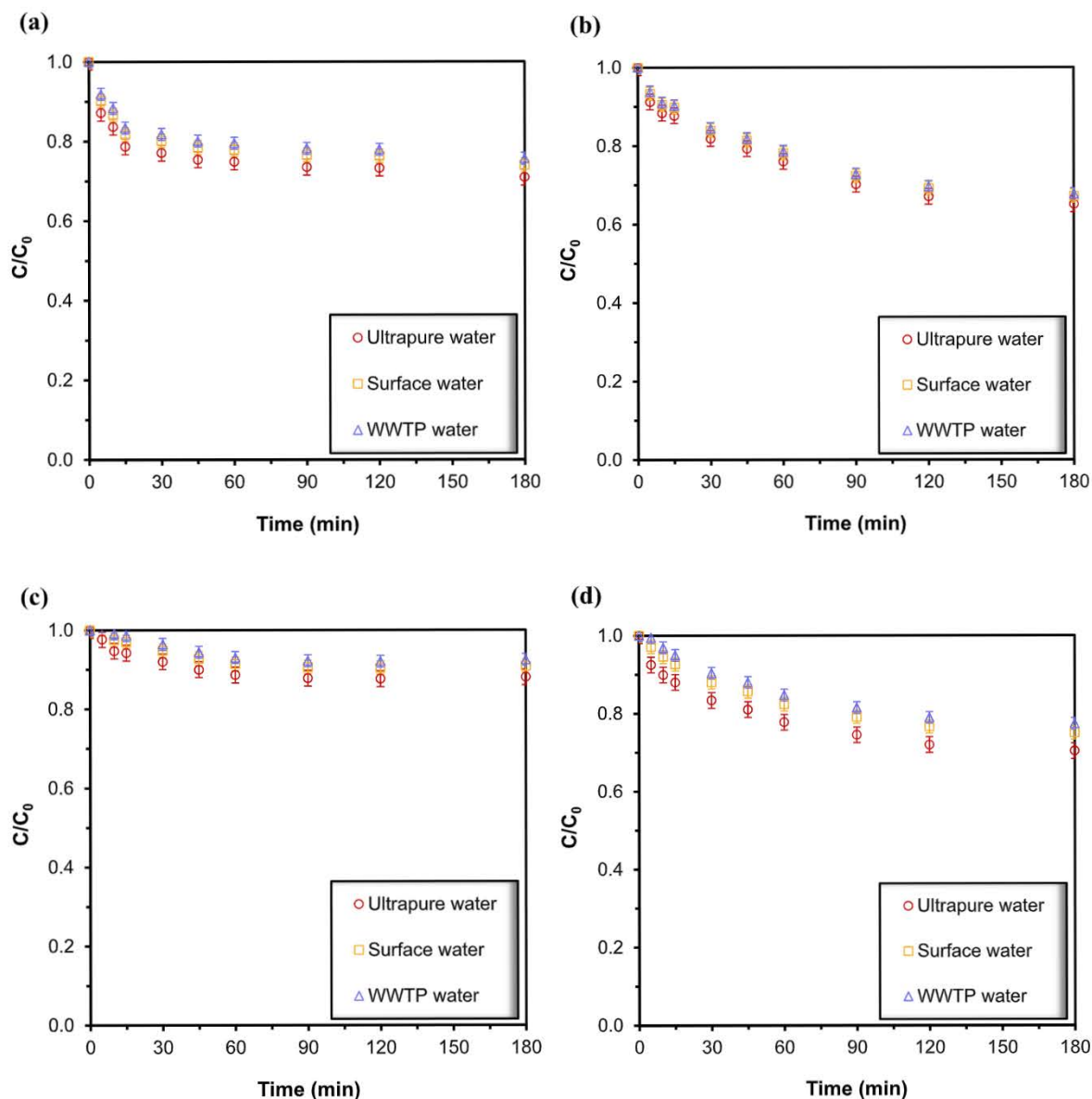
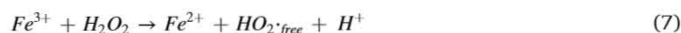
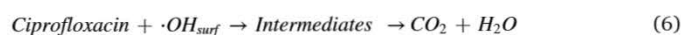
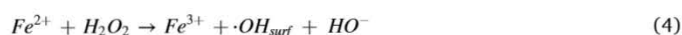
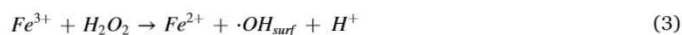


Fig. 5. Adsorption tests of the synthesized catalysts with different activating agents, sludge sources and aqueous matrices: Urban-Fe (a), Industrial-Fe (b), Industrial-Ni (c), Industrial-FeNi (d).

surface could accelerate the generation of $\bullet\text{OH}_{\text{surf}}$ from hydrogen peroxide through an intermolecular electron transfer process (Equations (3)-(4)). In addition, the oxygen-containing functional groups of the catalyst could react with hydrogen peroxide to form $\bullet\text{OH}_{\text{surf}}$ via electron transfer (Equation (5)) [89]. On the other hand, a small amount of leached ions could activate hydrogen peroxide to produce $\bullet\text{OH}_{\text{surf}}$ via chain reaction (Equations (7)-(8)). As a final step, the ciprofloxacin molecule could be degraded by the $\bullet\text{OH}_{\text{surf}}$ generated on the catalyst surface (Equations (6)) and a small part of $\bullet\text{OH}_{\text{free}}$ in the solution (Equation (9)). In this sense, the ciprofloxacin can be degraded indirectly through the oxidation of OH^- , and directly mediate electron transfer processes of the oxygen-containing functional groups and the metal of the catalyst. In addition, the carbon base can act as a medium for electron transfer from ciprofloxacin (as electron donor) to hydrogen peroxide (as electron acceptor) [90].



Ciprofloxacin degradation intermediates were identified by a Bruker LC-QTOF-MS Impact II instrument for each of the four catalysts used in this work. The possible molecular structure was proposed for each intermediate on the basis of MS/MS fragments and their m/z as shown in Tables S1-S4. MS/MS spectra or MS spectra of ciprofloxacin and intermediates are shown in Fig. S3-S6. In addition, energy data and cartesian coordinates for the optimised structure of the organic compounds involved in the reactions are given in Supplementary Material (Table S5-S23). Based on the Fukui index and in conjunction with the identification of the intermediate products of the four catalysts, the different

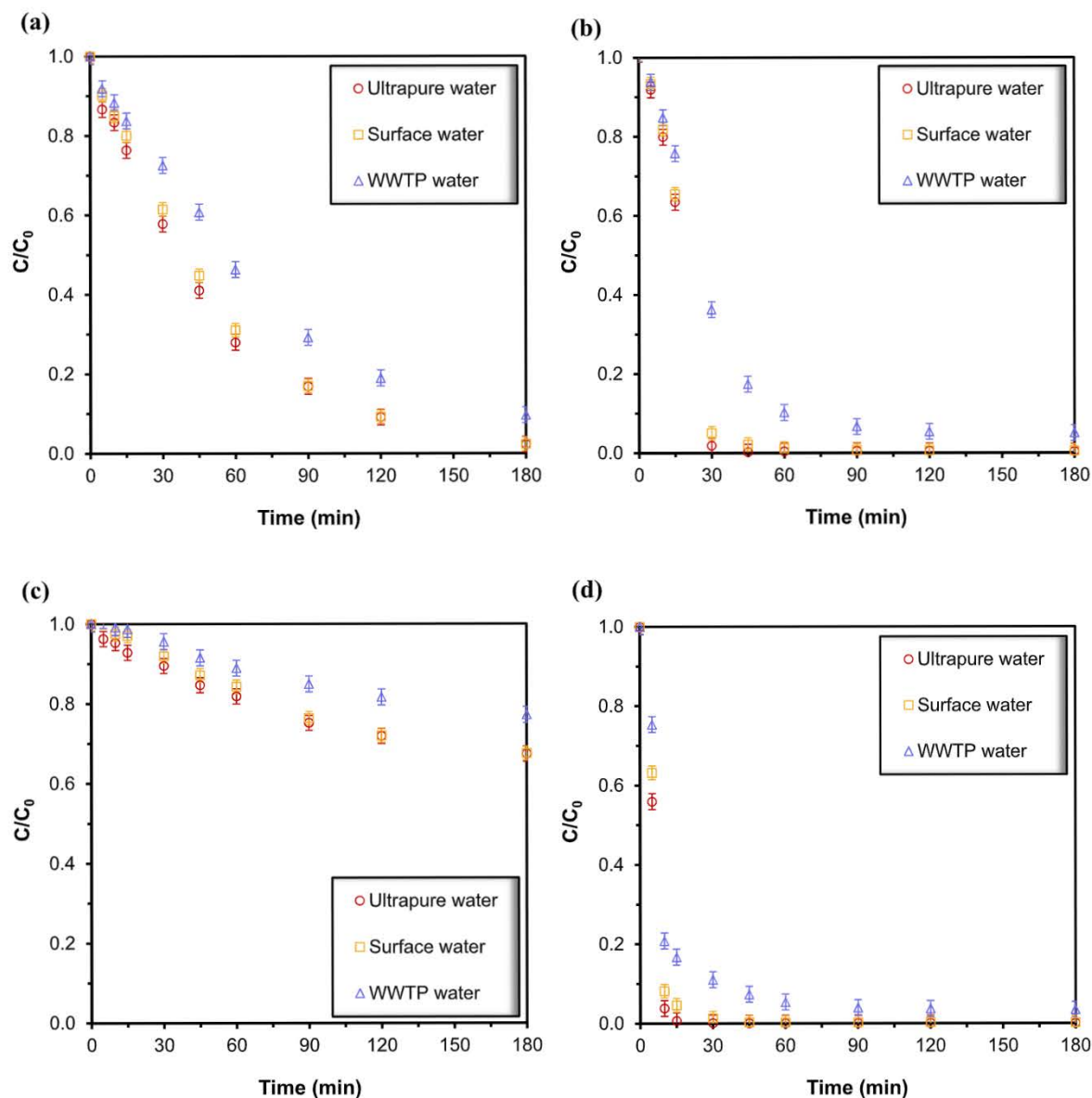


Fig. 6. Catalytic activity of the synthesized catalysts with different activating agents, sludge sources and aqueous matrices: Urban-Fe (a), Industrial-Fe (b), Industrial-Ni (c), Industrial-FeNi (d).

Table 6

Initial reaction rates of the synthesized catalysts with different activating agents, sludge sources and aqueous matrices.

	Urban-Fe	Industrial-Fe	Industrial-Ni	Industrial-FeNi
r_0 , Ultrapure water ($\text{mg}_{\text{Ciprofloxacin}}/\text{g}_{\text{Catalyst}} \cdot \text{min}$)	2.59	3.82	1.07	12.61
r_0 , surface water ($\text{mg}_{\text{Ciprofloxacin}}/\text{g}_{\text{Catalyst}} \cdot \text{min}$)	2.16	2.79	0.29	10.53
r_0 , WWTP water ($\text{mg}_{\text{Ciprofloxacin}}/\text{g}_{\text{Catalyst}} \cdot \text{min}$)	2.02	2.32	0.16	7.05

possible degradation pathways of ciprofloxacin in each system were proposed (T1-T4), taking into account the integration of the degradation pathways of all catalysts, as shown in Figs. 7-10. The Fukui index (f^0) was computed to identify the vulnerable atomic sites of the ciprofloxacin molecule for radical attack (Fig. 11a,b). According to Fukui function

(Eq. 2), a high f^- value suggests that an atom is more likely to be attacked by electrophilic reagent (nucleophilic reaction), and a high f^0 value indicates that an atom is likely to be attacked by $\bullet\text{OH}$. The 1(C), 3(C), 5(C), 11(F), 15(O), 19(N), 20(C), 35(H) and 41(H) positions exhibited high f^- values, suggesting the potential electrophilic attack. The 6(C), 8(C), 10(C) and 15(O) positions displayed high positive point charges, and so these positions are expected to undergo preferential nucleophilic attack. High f^0 values were calculated for the 3(C), 6(C), 10(C), 15(O), and 19(N) positions, indicating that these regions tend to lose electrons and be attacked by $\bullet\text{OH}$.

The possible degradation reactions of ciprofloxacin could follow four different degradation pathways (Fig. 7). In the first one, compounds with $m/z = 330$, 346 and 261 are formed by processes of defluorination and hydroxylation, followed by the cleavage of piperazine ring. All these processes have been reported in the degradation of fluoroquinolones [91,92]. In the second pathway, hydroxyl groups are incorporated into the piperazine ring and subsequently oxidised. Successive CO losses could lead to the opening and disappearance of the piperazine ring, resulting in formation of the compound with $m/z = 263$. The third

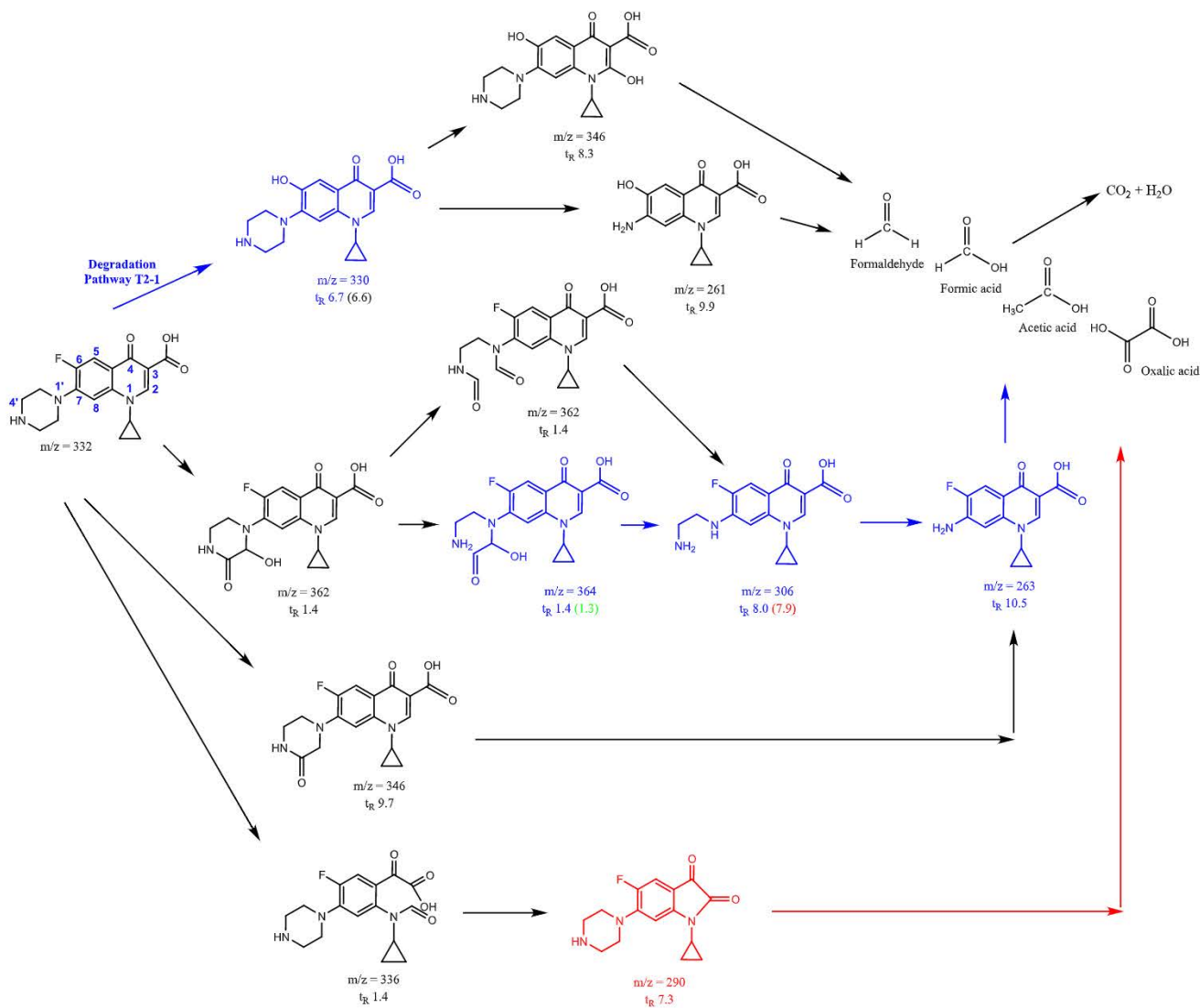


Fig. 7. Degradation pathway of ciprofloxacin by T1 (Urban-Fe) comprising T2 (Industrial-Fe), part of T3 (Industrial-Ni) and part of T4 (Industrial FeNi).

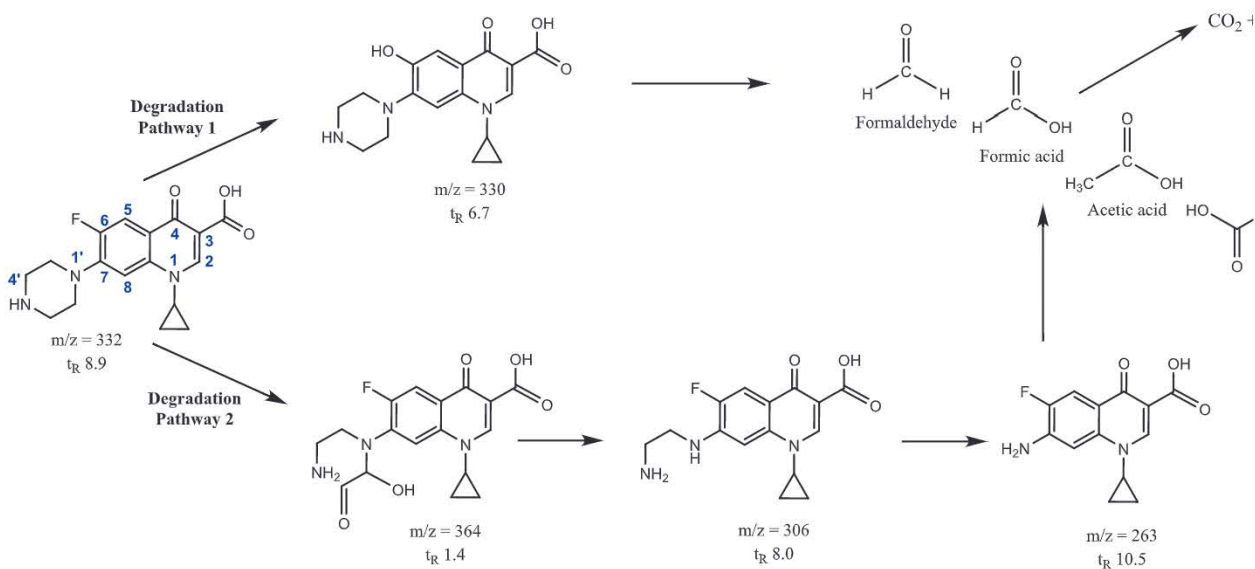


Fig. 8. Degradation pathway of ciprofloxacin by T2 (Industrial-Fe).

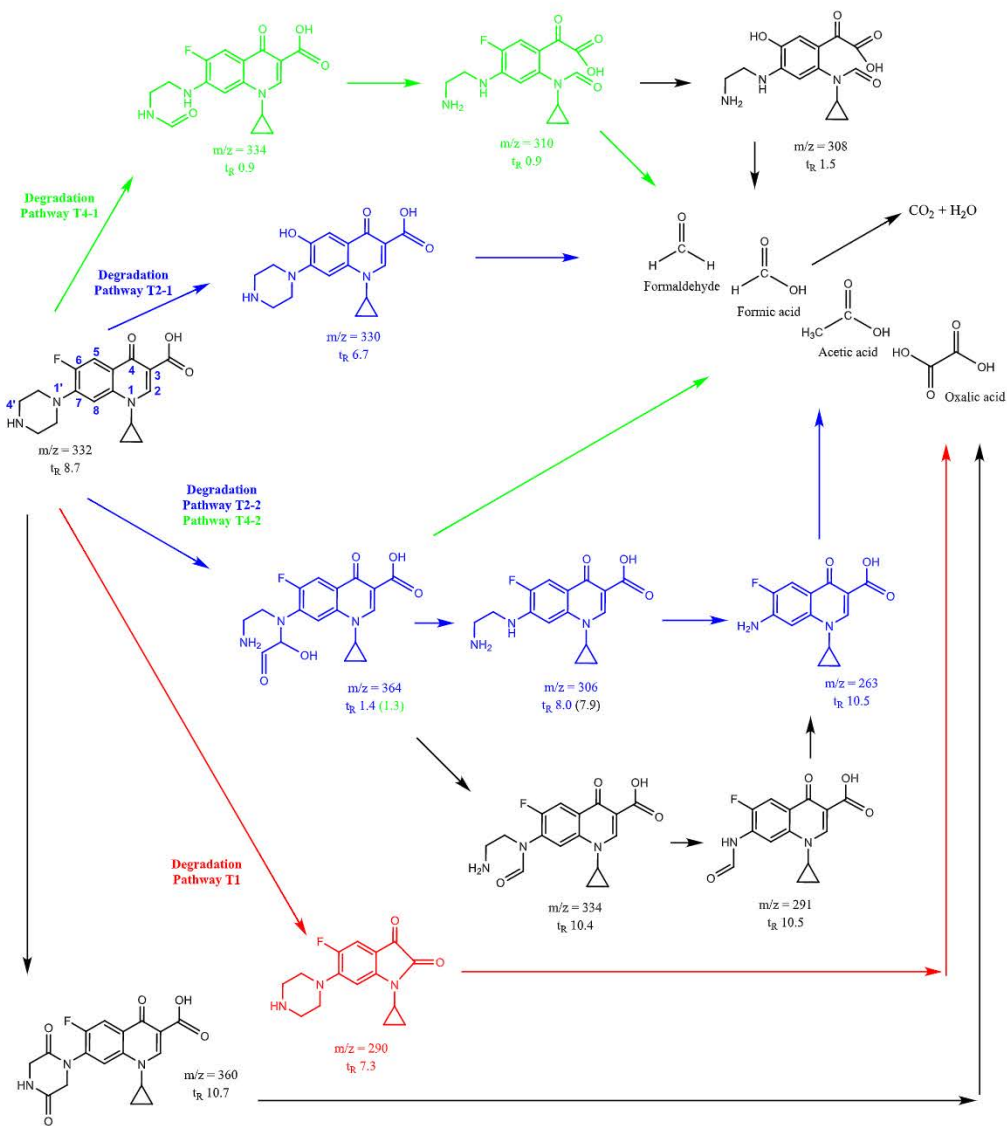


Fig. 9. Degradation pathway of ciprofloxacin by T3 (Industrial-Ni) from T2 (Industrial-Fe) as contained in T1 (Urban-Fe) and T4 (Industrial-FeNi).

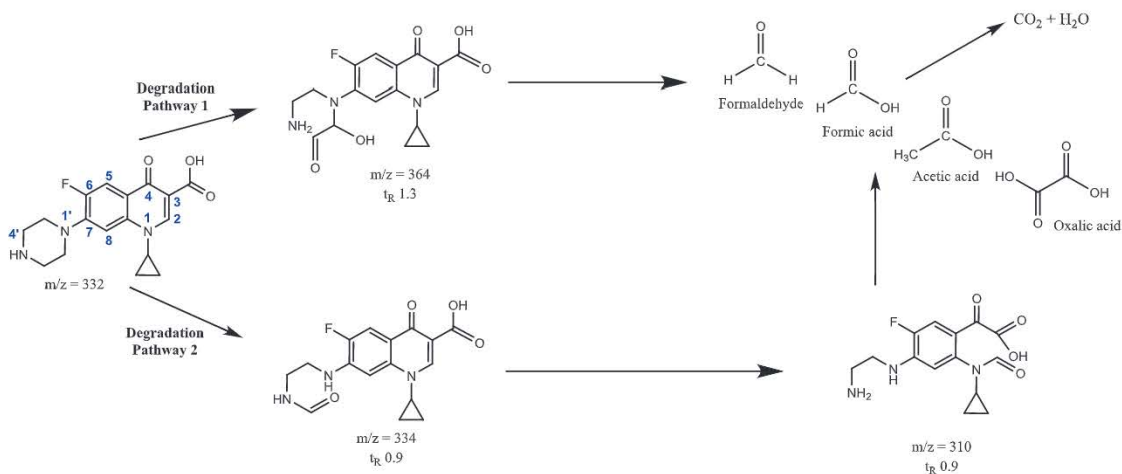
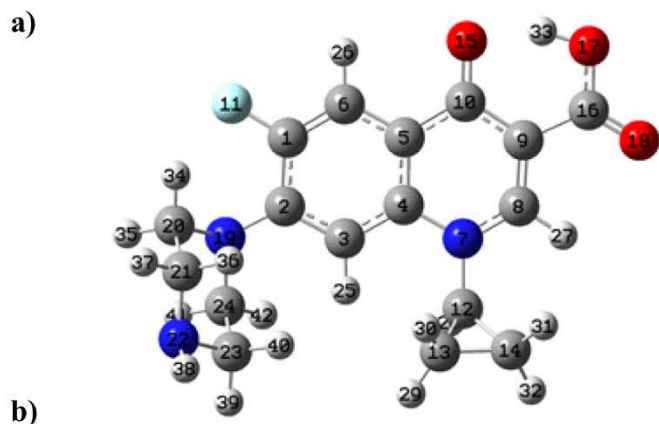


Fig. 10. Degradation pathway of ciprofloxacin by T4 (Industrial-FeNi).



Atom	q(N)	q(N+1)	q(N-1)	f ⁻	f ⁺	f ⁰
1(C)	0,0820	0,0395	0,1287	0,0467	0,0424	0,0446
2(C)	0,0506	-0,0058	0,0820	0,0314	0,0564	0,0439
3(C)	-0,0625	-0,1071	0,0115	0,0740	0,0446	0,0593
4(C)	0,0562	0,0276	0,0778	0,0216	0,0287	0,0251
5(C)	-0,0376	-0,0659	0,0227	0,0603	0,0283	0,0443
6(C)	-0,0449	-0,1206	-0,0154	0,0296	0,0756	0,0526
7(N)	0,0319	-0,0082	0,0384	0,0065	0,0400	0,0233
8(C)	0,0802	-0,0051	0,0974	0,0172	0,0853	0,0512
9(C)	-0,0678	-0,1006	-0,0523	0,0155	0,0328	0,0242
10(C)	0,1133	0,0015	0,1326	0,0192	0,1118	0,0655
11(F)	-0,0987	-0,1198	-0,0729	0,0258	0,0211	0,0234
12(C)	0,0262	0,0190	0,0278	0,0016	0,0072	0,0044
13(C)	-0,0588	-0,0676	-0,0557	0,0031	0,0088	0,0059
14(C)	-0,0557	-0,0640	-0,0516	0,0040	0,0084	0,0062
15(O)	-0,3113	-0,4147	-0,2815	0,0297	0,1035	0,0666
16(C)	0,1831	0,1669	0,1902	0,0071	0,0163	0,0117
17(O)	-0,2278	-0,2443	-0,2204	0,0074	0,0165	0,0120
18(O)	-0,3824	-0,4060	-0,3715	0,0108	0,0236	0,0172
19(N)	-0,0700	-0,0934	0,0960	0,1660	0,0233	0,0947
20(C)	-0,0088	-0,0171	0,0223	0,0311	0,0082	0,0197
21(C)	-0,0155	-0,0199	0,0108	0,0263	0,0044	0,0154
22(N)	-0,1762	-0,1789	-0,1527	0,0235	0,0026	0,0131
23(C)	-0,0136	-0,0175	0,0117	0,0253	0,0039	0,0146
24(C)	-0,0032	-0,0099	0,0265	0,0297	0,0067	0,0182
25(H)	0,0510	0,0334	0,0729	0,0219	0,0176	0,0198
26(H)	0,0598	0,0214	0,0777	0,0180	0,0384	0,0282
27(H)	0,0748	0,0394	0,0831	0,0083	0,0355	0,0219
28(H)	0,0673	0,0524	0,0716	0,0043	0,0149	0,0096
29(H)	0,0588	0,0519	0,0617	0,0030	0,0069	0,0049
30(H)	0,0543	0,0476	0,0573	0,0030	0,0068	0,0049
31(H)	0,0594	0,0520	0,0620	0,0026	0,0074	0,0050
32(H)	0,0599	0,0535	0,0626	0,0028	0,0063	0,0045
33(H)	0,1100	0,0955	0,1148	0,0048	0,0145	0,0096
34(H)	0,0360	0,0297	0,0586	0,0225	0,0064	0,0145
35(H)	0,0378	0,0299	0,0712	0,0334	0,0078	0,0206
36(H)	0,0254	0,0208	0,0439	0,0185	0,0046	0,0115
37(H)	0,0447	0,0397	0,0679	0,0232	0,0050	0,0141
38(H)	0,1100	0,1071	0,1294	0,0193	0,0030	0,0111
39(H)	0,0444	0,0398	0,0665	0,0221	0,0047	0,0134
40(H)	0,0280	0,0241	0,0456	0,0175	0,0039	0,0107
41(H)	0,0397	0,0312	0,0754	0,0357	0,0085	0,0221
42(H)	0,0506	0,0437	0,0762	0,0256	0,0069	0,0162

Fig. 11. Ciprofloxacin chemical structure (a). Hirshfeld charges and condensed Fukui functions of ciprofloxacin (b). Units used are “e” (elementary charge).

pathway involved the oxidation of the piperazine ring ($m/z = 346$), and subsequent loss of this ring generates the compound $m/z = 263$ [93]. Finally, in the fourth pathway, it is proposed that the intermediate with $m/z = 336$ could be generated by the attack of free radicals on $C=C$ followed by the loss of CO. A compound with $m/z = 290$ could be formed through a decarboxylation process, where later an intramolecular

nucleophilic substitution reaction takes place.

4. Conclusions

This work addressed the valorisation of sewage sludge by pyrolytic processes to produce iron and nickel carbonaceous catalysts that may be applied in the removal of emerging pollutants, such as the antibiotic ciprofloxacin. In this regard, the use of sewage sludge as a biomass precursor promoted the generation of functional groups, as evidenced by both the chemical composition and the FTIR spectra. All materials exhibited a combination of Type I-IV N_2 adsorption-desorption isotherms, showing H3-H4 Type hysteresis loops. The average pore width of the materials was found in the mesopore zone, although they also presented a high microporosity, except for the catalyst obtained with nickel chloride as activating agent. S_{BET} values of the synthesized catalysts ranged from 397 to 713 m^2/g .

The adsorption blanks showed adsorption capacity values in the range of 40.4–73.9 mg/g, with the Industrial-Ni catalyst exhibiting the lowest value. Nickel, as active phase, also showed significantly low catalytic activity compared to iron. Although the bimetallic catalyst Industrial-FeNi had a higher iron content than Industrial-Fe and therefore a higher catalytic activity, the measured metal leaching into the reaction medium was higher. Consequently, the use of iron chloride as activating agent was preferable.

The experiments performed, as well as the DFT calculations developed, show that the active atoms of the ciprofloxacin molecule with high Fukui index indicate C-F bond cleavage, ring hydroxylation, nucleophilic addition and aldehydic reaction under radical attack.

5. Data availability

Data will be made available on request.

CRediT authorship contribution statement

Pablo Gutiérrez-Sánchez: Conceptualization, Investigation, Formal analysis, Software, Methodology, Writing – original draft, Writing – review & editing. **Silvia Álvarez-Torrellas:** Writing – review & editing. **Marcos Larriba:** Writing – review & editing. **M. Victoria Gil:** Software, Writing – review & editing. **Juan M. Garrido-Zoido:** Software, Writing – review & editing. **Juan García:** Conceptualization, Funding acquisition, Project administration, Writing – review & editing.

Declaration of Competing Interest

The authors declare that they have no known competing financial interests or personal relationships that could have appeared to influence the work reported in this paper.

Data availability

Data will be made available on request.

Acknowledgments

This work has been supported by the Spanish MICINN through the project CATAD3.0 PID2020-116478RB-I00. In addition, the authors thank the financial support from the Comunidad de Madrid (Spain) through the Industrial PhD projects (IND2017/AMB-7720 and IND2019/AMB-17114), REMTAVARES Network (S2018/EMT-4341) and the European Social Fund. MVG also thanks Grant PID2021-125295OB-I00 funded by MCIN/AEI/ 10.13039/501100011033 and by “ERDF A way of making Europe” and the Junta de Extremadura and the European Regional Development Fund (ERDF/FEDER), through Grant No. GR21039. The authors are grateful for the Supercomputer facility LUSITANIA funded by CenitS and the Computaex Foundation.

Appendix A. Supplementary material

Supplementary data to this article can be found online at <https://doi.org/10.1016/j.molliq.2023.121840>.

References

- [1] Y. Chen, J. Zhang, H. Xu, Exploration of the degradation mechanism of ciprofloxacin in water by nano zero-valent iron combined with activated carbon and nickel, *J. Mol. Liq.* 345 (2022), 118212, <https://doi.org/10.1016/J.MOLLIQ.2021.118212>.
- [2] Y. Qin, K. Wang, Q. Xia, S. Yu, M. Zhang, Y. An, X. Zhao, Z. Zhou, Up-concentration of nitrogen from domestic wastewater: A sustainable strategy from removal to recovery, *Chem. Eng. J.* 451 (2023), 138789, <https://doi.org/10.1016/J.CEJ.2022.138789>.
- [3] S.A. Afolalu, O.M. Ikumapayi, T.S. Ogedengbe, R.A. Kazeem, A.T. Ogundipe, Waste pollution, wastewater and effluent treatment methods - An overview, *Mater. Today.. Proc.* 62 (2022) 3282–3288, <https://doi.org/10.1016/J.MATPR.2022.04.231>.
- [4] P. Gutiérrez-Sánchez, P. Navarro, S. Álvarez-Torrellas, J. García, M. Larriba, Extraction of neonicotinoid pesticides from aquatic environmental matrices with sustainable terpenoids and eutectic solvents, *Sep. Purif. Technol.* 302 (2022), 122148, <https://doi.org/10.1016/J.SEPUR.2022.122148>.
- [5] O.J. Ajala, J.O. Tijani, R.B. Salau, A.S. Abdulkareem, O.S. Aremu, A review of emerging micro-pollutants in hospital wastewater: Environmental fate and remediation options, *Results Eng.* 16 (2022), 100671, <https://doi.org/10.1016/J.RINENG.2022.100671>.
- [6] J. Wilkinson, P.S. Hooda, J. Barker, J. Swinden, Occurrence, fate and transformation of emerging contaminants in water: An overarching review of the field, *Environ. Pollut.* 231 (2017) 954–970, <https://doi.org/10.1016/J.ENVPOL.2017.08.032>.
- [7] A. Pal, K.Y.H. Gin, A.Y.C. Lin, M. Reinhard, Impacts of emerging organic contaminants on freshwater resources: Review of recent occurrences, sources, fate and effects, *Sci. Total Environ.* 408 (2010) 6062–6069, <https://doi.org/10.1016/J.SCITOTENV.2010.09.026>.
- [8] K. Kümmerer, Antibiotics in the aquatic environment - A review - Part I, *Chemosphere* 75 (2009) 417–434, <https://doi.org/10.1016/J.CHEMOSPHERE.2008.11.086>.
- [9] F.S. Souza, L.A. Féris, Consumption-based approach for pharmaceutical compounds in a large hospital, *Doi: 10.1080/09593330.2016.1255262*. 38 (2016) 2217–2223. [Doi: 10.1080/09593330.2016.1255262](https://doi.org/10.1080/09593330.2016.1255262).
- [10] M. Ibáñez, L. Bijlsma, E. Pitarch, F.J. López, F. Hernández, Occurrence of pharmaceutical metabolites and transformation products in the aquatic environment of the Mediterranean area, *Trends Environ. Anal. Chem.* 29 (2021) e00118.
- [11] P. Sukul, M. Spittler, Fluoroquinolone antibiotics in the environment, *Rev. Environ. Contam. Toxicol.* 191 (2007) 131–162, https://doi.org/10.1007/978-0-387-69163-3_5.
- [12] M.S. Gaballah, J. Guo, H. Sun, D. Aboagye, M. Sobhi, A. Muhmood, R. Dong, A review targeting veterinary antibiotics removal from livestock manure management systems and future outlook, *Bioresour. Technol.* 333 (2021), 125069, <https://doi.org/10.1016/J.BIORTECH.2021.125069>.
- [13] C.F. Nnadozie, S. Kumari, F. Bux, Status of pathogens, antibiotic resistance genes and antibiotic residues in wastewater treatment systems, *Rev. Environ. Sci. Bio/ Technol.* 2017 16:3. 16 (2017) 491–515. [Doi: 10.1007/S11157-017-9438-X](https://doi.org/10.1007/S11157-017-9438-X).
- [14] D. Cheng, H.H. Ngo, W. Guo, S.W. Chang, D.D. Nguyen, Y. Liu, Q. Wei, D. Wei, A critical review on antibiotics and hormones in swine wastewater: Water pollution problems and control approaches, *J. Hazard. Mater.* 387 (2020), 121682, <https://doi.org/10.1016/J.JHAZMAT.2019.121682>.
- [15] L.J.M. Githinji, M.K. Musey, R.O. Ankumah, Evaluation of the fate of ciprofloxacin and amoxicillin in domestic wastewater, *Water Air Soil Pollut.* 219 (2011) 191–201, <https://doi.org/10.1007/S11270-010-0697-1/FIGURES/10>.
- [16] S. Aleksić, A.Ž. Gotvajn, K. Premzl, M. Kolar, S.Š. Turk, Ozonation of amoxicillin and ciprofloxacin in model hospital wastewater to increase biotreatability, *Antibiotics (Basel)*. 10 (2021), <https://doi.org/10.3390/ANTIBIOTICS10111407>.
- [17] S. Álvarez-Torrellas, J.A. Peres, V. Gil-Álvarez, G. Ovejero, J. García, Effective adsorption of non-biodegradable pharmaceuticals from hospital wastewater with different carbon materials, *Chem. Eng. J.* 320 (2017) 319–329, <https://doi.org/10.1016/j.cej.2017.03.077>.
- [18] Y. Segura, A. Cruz del Álamo, M. Munoz, S. Álvarez-Torrellas, J. García, J.A. Casas, Z.M. de Pedro, F. Martínez, A comparative study among catalytic wet air oxidation, Fenton, and Photo-Fenton technologies for the on-site treatment of hospital wastewater, *J. Environ. Manage.* 290 (2021), 112624, <https://doi.org/10.1016/J.JENVMAN.2021.112624>.
- [19] G. di Giacomo, P. Romano, Evolution and prospects in managing sewage sludge resulting from municipal wastewater purification, *Energies* 2022, Vol. 15, Page 5633. 15 (2022) 5633. [Doi: 10.3390/EN15155633](https://doi.org/10.3390/EN15155633).
- [20] J.C. Jiménez, J.G. Rodríguez, B.H. Mendioroz, V. Ismael Águeda Maté, S. Álvarez-Torrellas, Revision of the Most Harmful Organic Compounds Present in Sewage and Sludge, in: *The Handbook of Environmental Chemistry*, Springer, 2022: pp. 1–20. [Doi: 10.1007/978-94-007-855-5](https://doi.org/10.1007/978-94-007-855-5).
- [21] K. Shanmugam, V. Gadhamshetty, M. Tyskind, D. Bhattacharyya, V.K. K. Upadhyayula, A sustainable performance assessment framework for circular management of municipal wastewater treatment plants, *J. Clean. Prod.* 339 (2022), 130657, <https://doi.org/10.1016/J.JCLEPRO.2022.130657>.
- [22] Z. He, X. Cheng, G.Z. Kyzas, J. Fu, Pharmaceuticals pollution of aquaculture and its management in China, *J. Mol. Liq.* 223 (2016) 781–789, <https://doi.org/10.1016/J.MOLLIQ.2016.09.005>.
- [23] H. Zhang, F. Chen, J. Zhang, Y. Han, Supercritical water gasification of fuel gas production from waste lignin: The effect mechanism of different oxidized iron-based catalysts, *Int. J. Hydrogen Energy* 46 (2021) 30288–30299, <https://doi.org/10.1016/J.IJHYDENE.2021.06.169>.
- [24] H. Zhang, F. Chen, J. Xu, J. Zhang, Y. Han, Chemical reactions of oily sludge catalyzed by iron oxide under supercritical water gasification condition, *Front. Chem. Sci. Eng.* 16 (2022) 886–896, <https://doi.org/10.1007/S11705-021-2125-Z/METRICS>.
- [25] Z. Li, Y. Huang, Z. Zhu, H. Cheng, J. Zhao, M. Yu, W. Xu, Q. Yuan, T. He, S. Wang, Co-pyrolysis of sewage sludge with polyvinyl chloride (PVC)/CaO: Effects on heavy metals behavior and ecological risk, *Fuel* 333 (2023), 126281, <https://doi.org/10.1016/J.FUEL.2022.126281>.
- [26] J. Racek, J. Sevcik, T. Chorazy, J. Kucerik, P. Hlavinek, Biochar - recovery material from pyrolysis of sewage sludge: A review, *Waste Biomass Valoriz.* 11 (2020) 3677–3709, <https://doi.org/10.1007/S12649-019-00679-W/TABLES/16>.
- [27] I.B.S. Poblete, O. de Q.F. Araujo, J.L. de Medeiros, Sewage-water treatment and sewage-sludge management with power production as bioenergy with carbon capture system: A review, *Processes* 2022, Vol. 10, Page 788. 10 (2022) 788. [Doi: 10.3390/PR10040788](https://doi.org/10.3390/PR10040788).
- [28] X. Chen, S. Jeyaseelan, N. Graham, Physical and chemical properties study of the activated carbon made from sewage sludge, *Waste Manag.* 22 (2002) 755–760, [https://doi.org/10.1016/S0956-053X\(02\)00057-0](https://doi.org/10.1016/S0956-053X(02)00057-0).
- [29] E. Sanz-Santos, S. Álvarez-Torrellas, M. Larriba, J. García, Activated carbons derived from biomass for the removal by adsorption of several pesticides from water, *Advanced Materials for Sustainable Environmental Remediation: Terrestrial and Aquatic Environments*. (2022) 565–583. [Doi: 10.1016/B978-0-323-90485-8.00020-5](https://doi.org/10.1016/B978-0-323-90485-8.00020-5).
- [30] E. Sanz-Santos, S. Álvarez-Torrellas, M. Larriba, D. Calleja-Cascajero, J. García, Enhanced removal of neonicotinoid pesticides present in the Decision 2018/840/EU by new sewage sludge-based carbon materials, *J. Environ. Manage.* 313 (2022), 115020.
- [31] N. Graham, X.G. Chen, S. Jayaseelan, The potential application of activated carbon from sewage sludge to organic dyes removal, *Water Sci. Technol.* 43 (2001) 245–252, <https://doi.org/10.2166/WST.2001.0096>.
- [32] Y. Huacalco-Aguilar, S. Álvarez-Torrellas, M.v. Gil, M. Larriba, J. García, Insights of emerging contaminants removal in real water matrices by CWPO using a magnetic catalyst, *J. Environ. Chem. Eng.* 9 (2021), 106321, <https://doi.org/10.1016/J.JECE.2021.106321>.
- [33] A. Pieczyńska, A.F. Borzyszkowska, A. Ofiarska, E.M. Siedlecka, Removal of cytostatic drugs by AOPs: A review of applied processes in the context of green, *technology* 47 (2017) 1282–1335, <https://doi.org/10.1080/10643389.2017.1370990>.
- [34] N. Nasrollahi, V. Vatanpour, A. Khataee, Removal of antibiotics from wastewaters by membrane technology: Limitations, successes, and future improvements, *Sci. Total Environ.* 838 (2022), 156010, <https://doi.org/10.1016/J.SCITOTENV.2022.156010>.
- [35] V. Homem, L. Santos, Degradation and removal methods of antibiotics from aqueous matrices - A review, *J. Environ. Manage.* 92 (2011) 2304–2347, <https://doi.org/10.1016/J.JENVMAN.2011.05.023>.
- [36] G. Lofrano, R. Pedrazzani, G. Libralato, M. Carotenuto, Advanced oxidation processes for antibiotics removal: a review, *Curr. Org. Chem.* 21 (2017) 1054–1067.
- [37] M. Verma, A.K. Haritash, Review of advanced oxidation processes (AOPs) for treatment of pharmaceutical wastewater, *Adv. Environ. Res.* 9 (2020) 1–17.
- [38] R. Anjali, S. Shanthakumar, Insights on the current status of occurrence and removal of antibiotics in wastewater by advanced oxidation processes, *J. Environ. Manage.* 246 (2019) 51–62, <https://doi.org/10.1016/J.JENVMAN.2019.05.090>.
- [39] M. Malakootian, M. Faraji, M. Malakootian, M. Nozari, M. Malakootian, Ciprofloxacin removal from aqueous media by adsorption process: A systematic review and meta-analysis, *Desalin. Water Treat.* 229 (2021) 252–282.
- [40] C.E. Enyoh, Q. Wang, Adsorption of ciprofloxacin from aqueous solution by plastic-based adsorbents: a review, *International Journal of Environmental Analytical Chemistry* 1-21 (2022), <https://doi.org/10.1080/03067319.2022.2106432>.
- [41] M. Malakootian, M. Yaseri, M. Faraji, Removal of antibiotics from aqueous solutions by nanoparticles: a systematic review and meta-analysis, *Environ. Sci. Pollut. Res.* 2019 26:9. 26 (2019) 8444–8458. [Doi: 10.1007/S11356-019-04227-W](https://doi.org/10.1007/S11356-019-04227-W).
- [42] American Public Health Association, Standard methods for the examination of water and wastewater, 23rd ed., 2017.
- [43] A.G. Gonçalves, J.J.M. Orfão, M.F.R. Pereira, Catalytic ozonation of sulphamethoxazole in the presence of carbon materials: Catalytic performance and reaction pathways, *J. Hazard. Mater.* 239–240 (2012) 167–174, <https://doi.org/10.1016/j.jhazmat.2012.08.057>.
- [44] F.J. Beltrán, A. Aguinaco, J.F. García-Araya, A. Oropesa, Ozone and photocatalytic processes to remove the antibiotic sulfamethoxazole from water, *Water Res.* 42 (2008) 3799–3808, <https://doi.org/10.1016/j.watres.2008.07.019>.
- [45] A.G. Trovó, R.F. Pupo Nogueira, A. Agüera, A.R. Fernandez-Alba, S. Malato, Degradation of the antibiotic amoxicillin by photo-Fenton process - Chemical and toxicological assessment, *Water Res.* 45 (2011) 1394–1402, <https://doi.org/10.1016/j.watres.2010.10.029>.
- [46] A. Ledezma Estrada, Y.Y. Li, A. Wang, Biodegradability enhancement of wastewater containing cefalexin by means of the electro-Fenton oxidation process,

- J. Hazard. Mater. 227–228 (2012) 41–48, <https://doi.org/10.1016/j.jhazmat.2012.04.079>.
- [47] T.H. Kim, S.D. Kim, H.Y. Kim, S.J. Lim, M. Lee, S. Yu, Degradation and toxicity assessment of sulfamethoxazole and chlortetracycline using electron beam, ozone and UV, J. Hazard. Mater. 227–228 (2012) 237–242, <https://doi.org/10.1016/j.jhazmat.2012.05.038>.
- [48] D. Rodríguez-Llorente, E. Hernández, P. Gutiérrez-Sánchez, P. Navarro, V. Ismael Águeda, S. Álvarez-Torrellas, J. García, M. Larriba, Extraction of pharmaceuticals from hospital wastewater with eutectic solvents and terpenoids: Computational, experimental, and simulation studies, Chem. Eng. J. 451 (2023), 138544, <https://doi.org/10.1016/J.CEJ.2022.138544>.
- [49] P. Gutiérrez-Sánchez, D. Rodríguez-Llorente, P. Navarro, V.I. Águeda, S. Álvarez-Torrellas, J. García, M. Larriba, Extraction of antibiotics identified in the EU Watch List 2020 from hospital wastewater using hydrophobic eutectic solvents and terpenoids, Sep. Purif. Technol. 282 (2022), 120117, <https://doi.org/10.1016/j.seppur.2021.120117>.
- [50] P. Gutiérrez-Sánchez, S. Álvarez-Torrellas, M. Larriba, M.V. Gil, J.M. Garrido-Zoido, J. García, Efficient removal of antibiotic ciprofloxacin by catalytic wet air oxidation using sewage sludge-based catalysts: Degradation mechanism by DFT studies, J. Environ. Chem. Eng. 11 (2023), 109344, <https://doi.org/10.1016/J.JECE.2023.109344>.
- [51] F. Weinhold, C.R. Landis, Discovering chemistry with natural bond orbitals, Discovering Chem. with Nat. Bond Orbitals (2012), <https://doi.org/10.1002/9781118229101>.
- [52] E.D. Glendening, A.E. Reed, J.E. Carpenter, F. Weinhold, NBO Version 3.1, TCI, University of Wisconsin. 65 (1998).
- [53] A.V. Marenich, C.J. Cramer, D.G. Truhlar, Universal solvation model based on solute electron density and on a continuum model of the solvent defined by the bulk dielectric constant and atomic surface tensions, J. Phys. Chem. B. 113 (2009) 6378–6396. Doi: 10.1021/JP810292N/SUPPL_FILE/JP810292N_SI_003.PDF.
- [54] R. Dennington, T. Keith, J. Millam, GaussView, Version 6, Semichem Inc., Shawnee Mission, KS. (2016).
- [55] R.G. Parr, W. Yang, Density Functional Approach to the Frontier-Electron Theory of Chemical Reactivity, J. Am. Chem. Soc. 106 (1984) 4049–4050, <https://doi.org/10.1021/JA00326A036/ASSET/JA00326A036.FP.PNG.V03>.
- [56] J. Jgawe, P.W. Olupot, E. Menya, H.M. Kalibbala, Synthesis and application of granular activated carbon from biomass waste materials for water treatment: A review, J. Bioresour. Bioproducts 6 (2021) 292–322, <https://doi.org/10.1016/J.JOBAB.2021.03.003>.
- [57] G. Gascó, C.G. Blanco, F. Guerrero, A.M.M. Lázaro, The influence of organic matter on sewage sludge pyrolysis, J. Anal. Appl. Pyrol. 74 (2005) 413–420, <https://doi.org/10.1016/J.JAAP.2004.08.007>.
- [58] M.J. Martin, E. Serra, A. Ros, M.D. Balaguer, M. Rigola, Carbonaceous adsorbents from sewage sludge and their application in a combined activated sludge-powdered activated carbon (AS-PAC) treatment, Carbon N Y. 42 (2004) 1389–1394, <https://doi.org/10.1016/J.CARBON.2004.01.011>.
- [59] K.H. Lin, N. Lai, J.Y. Zeng, H.L. Chiang, Residue characteristics of sludge from a chemical industrial plant by microwave heating pyrolysis, Environmental Science and Pollution, Research 25 (2018) 6487–6496, <https://doi.org/10.1007/S11356-017-1003-1/TABLES/4>.
- [60] E. Sanz-Santos, S. Álvarez-Torrellas, L. Ceballos, M. Larriba, V.I. Águeda, J. García, Application of sludge-based activated carbons for the effective adsorption of neonicotinoid pesticides, Appl. Sci. 11 (2021) 3087.
- [61] C. Huang, B.A. Mohamed, L.Y. Li, Comparative life-cycle assessment of pyrolysis processes for producing bio-oil, biochar, and activated carbon from sewage sludge, Resour. Conserv. Recycl. 181 (2022), 106273, <https://doi.org/10.1016/J.RESCONREC.2022.106273>.
- [62] C. Nieto-Delgado, M. Terrones, J.R. Rangel-Mendez, Development of highly microporous activated carbon from the alcoholic beverage industry organic by-products, Biomass Bioenergy 35 (2011) 103–112, <https://doi.org/10.1016/J.BIOMBIOE.2010.08.025>.
- [63] B. Janković, N. Manić, V. Dodevski, I. Radović, M. Pijović, Đ. Katnić, G. Tasić, Physico-chemical characterization of carbonized apricot kernel shell as precursor for activated carbon preparation in clean technology utilization, J. Clean. Prod. 236 (2019), 117614, <https://doi.org/10.1016/J.JCLEPRO.2019.117614>.
- [64] Q. Yin, M. Liu, H. Ren, Biochar produced from the co-pyrolysis of sewage sludge and walnut shell for ammonium and phosphate adsorption from water, J. Environ. Manage. 249 (2019), 109410, <https://doi.org/10.1016/J.JENVMAN.2019.109410>.
- [65] A. Gopinath, G. Divyapriya, V. Srivastava, A.R. Laiju P. v. Nidheesh, M.S. Kumar, Conversion of sewage sludge into biochar: A potential resource in water and wastewater treatment, Environ. Res. 194 (2021), 110656, <https://doi.org/10.1016/J.ENVRES.2020.110656>.
- [66] S. Jerez, M. Ventura, R. Molina, M.I. Pariente, F. Martínez, J.A. Melero, Comprehensive characterization of an oily sludge from a petrol refinery: A step forward for its valorization within the circular economy strategy, J. Environ. Manage. 285 (2021), 112124, <https://doi.org/10.1016/J.JENVMAN.2021.112124>.
- [67] R. Yin, W. Guo, H. Wang, J. Du, Q. Wu, J.S. Chang, N. Ren, Singlet oxygen-dominated peroxydisulfate activation by sludge-derived biochar for sulfamethoxazole degradation through a nonradical oxidation pathway: Performance and mechanism, Chem. Eng. J. 357 (2019) 589–599, <https://doi.org/10.1016/J.CEJ.2018.09.184>.
- [68] M. Thommes, K. Kaneko, A. v. Neimark, J.P. Olivier, F. Rodríguez-Reinoso, J. Rouquerol, K.S.W. Sing, Physisorption of gases, with special reference to the evaluation of surface area and pore size distribution (IUPAC Technical Report), Pure Appl. Chem. 87 (2015) 1051–1069.
- [69] Q. Chen, H. Liu, J.H. Ko, H. Wu, Q. Xu, Structure characteristics of bio-char generated from co-pyrolysis of wooden waste and wet municipal sewage sludge, Fuel Process. Technol. 183 (2019) 48–54, <https://doi.org/10.1016/J.FUPROC.2018.11.005>.
- [70] M. Kończak, P. Oleszczuk, K. Rózyło, Application of different carrying gases and ratio between sewage sludge and willow for engineered (smart) biochar production, J. CO2 Util. 29 (2019) 20–28, <https://doi.org/10.1016/J.JCOU.2018.10.019>.
- [71] T. Boualem, A. Debab, A. Martínez de Yuso, M.T. Izquierdo, Activated carbons obtained from sewage sludge by chemical activation: Gas-phase environmental applications, J. Environ. Manage. 140 (2014) 145–151, <https://doi.org/10.1016/J.JENVMAN.2014.03.016>.
- [72] C. Schlumberger, M. Thommes, Characterization of hierarchically ordered porous materials by physisorption and mercury porosimetry—A tutorial review, Adv. Mater. Interfaces 8 (2021) 2002181.
- [73] P. Maziarka, C. Wurzer, P.J. Arauzo, A. Dieguez-Alonso, O. Mašek, F. Ronsse, Do you BET on routine? The reliability of N2 physisorption for the quantitative assessment of biochar's surface area, Chem. Eng. J. 418 (2021), 129234, <https://doi.org/10.1016/J.CEJ.2021.129234>.
- [74] J. Rouquerol, P. Llewellyn, F. Rouquerol, Is the BET equation applicable to microporous adsorbents? Stud. Surf. Sci. Catal. 160 (2007) 49–56, [https://doi.org/10.1016/S0167-2991\(07\)80008-5](https://doi.org/10.1016/S0167-2991(07)80008-5).
- [75] J. Alvarez, G. Lopez, M. Amutio, J. Bilbao, M. Olazar, Preparation of adsorbents from sewage sludge pyrolytic char by carbon dioxide activation, Process Saf. Environ. Prot. 103 (2016) 76–86.
- [76] H. Saygılı, F. Güzel, Y. Önal, Conversion of grape industrial processing waste to activated carbon sorbent and its performance in cationic and anionic dyes adsorption, J. Clean. Prod. 93 (2015) 84–93, <https://doi.org/10.1016/j.jclepro.2015.01.009>.
- [77] A. Kumar, P. Kumar, C. Joshi, M. Manchanda, R. Boukherroub, S.L. Jain, Nickel Decorated on Phosphorous-Doped Carbon Nitride as an Efficient Photocatalyst for Reduction of Nitrobenzenes, Nanomaterials 2016, Vol. 6, Page 59. 6 (2016) 59. Doi: 10.3390/NANO6040059.
- [78] A.F.M. Streit, L.N. Côrtes, S.P. Druzian, M. Godinho, G.C. Collazzo, D. Perondi, G. L. Dotto, Development of high quality activated carbon from biological sludge and its application for dyes removal from aqueous solutions, Sci. Total Environ. 660 (2019) 277–287, <https://doi.org/10.1016/J.SCITOTENV.2019.01.027>.
- [79] L. Li, J. Ai, W. Zhang, S. Peng, T. Dong, Y. Deng, Y. Cui, D. Wang, Relationship between the physicochemical properties of sludge-based carbons and the adsorption capacity of dissolved organic matter in advanced wastewater treatment: Effects of chemical conditioning, Chemosphere 243 (2020), 125333, <https://doi.org/10.1016/J.CHEMOSPHERE.2019.125333>.
- [80] Q.H. Lin, H. Cheng, G.Y. Chen, Preparation and characterization of carbonaceous adsorbents from sewage sludge using a pilot-scale microwave heating equipment, J. Anal. Appl. Pyrol. 93 (2012) 113–119, <https://doi.org/10.1016/J.JAAP.2011.10.006>.
- [81] R. Ali, Z. Aslam, R.A. Shawabkeh, A. Asghar, I.A. Hussein Bet, FTIR, and RAMAN characterizations of activated carbon from waste oil fly ash, Turk. J. Chem. 44 (2020) 279–295, <https://doi.org/10.3906/kim-1909-20>.
- [82] L. Liu, Y. Lin, Y. Liu, H. Zhu, Q. He, Removal of methylene blue from aqueous solutions by sewage sludge based granular activated carbon: Adsorption equilibrium, kinetics, and thermodynamics, J. Chem. Eng. Data 58 (2013) 2248–2253, https://doi.org/10.1021/JE4003543/ASSET/IMAGES/LARGE/JE-2013-003543_0006.JPEG.
- [83] K. Fang, J. Chen, X. Zhou, C. Mei, Q. Tian, J. Xu, C.P. Wong, Decorating biomass-derived porous carbon with Fe2O3 ultrathin film for high-performance supercapacitors, Electrochim. Acta 261 (2018) 198–205, <https://doi.org/10.1016/J.JELECTACTA.2017.12.140>.
- [84] R. Fernández, J. Estelle, Y. Cesteros, P. Salagre, F. Medina, J.E. Sueiras, J.L. Garcia Fierro, Structural characterization of NiO doped with several caesium loadings, J. Mol. Catal. A Chem. 119 (1997) 77–85, [https://doi.org/10.1016/S1381-1169\(96\)00471-2](https://doi.org/10.1016/S1381-1169(96)00471-2).
- [85] W.K. Wakejo, B.T. Meshasha, J.W. Kang, Y. Chebude, Enhanced ciprofloxacin removal from aqueous solution using a chemically modified biochar derived from bamboo sawdust: Adsorption process optimization with response surface methodology, Adsorpt. Sci. Technol. 2022 (2022), <https://doi.org/10.1155/2022/2699530>.
- [86] Y. Fu, Z. Yang, Y. Xia, Y. Xing, X. Gui, Adsorption of ciprofloxacin pollutants in aqueous solution using modified waste grapefruit peel, Doi: 10.1080/15567036.2019.1624877. 43 (2019) 225–234. Doi: 10.1080/15567036.2019.1624877.
- [87] Q.T. Tran, T.H. Do, X.L. Ha, H.P. Nguyen, A.T. Nguyen, T.C.Q. Ngo, H.D. Chau, Study of the ciprofloxacin adsorption of activated carbon prepared from mangosteen peel, Appl. Sci. 2022, Vol. 12, Page 8770. 12 (2022) 8770. Doi: 10.3390/AP12178770.
- [88] M. N. A. Renita A. S. Kumar P. S. Abraham L. Adsorption of ciprofloxacin from aqueous solution using surface improved tamarind shell as an economical and effective adsorbent, Doi: 10.1080/15226514.2021.1932730. 24 (2021) 224–234. Doi: 10.1080/15226514.2021.1932730.
- [89] M. Munoz, P. Domínguez, Z.M. de Pedro, J.A. Casas, J.J. Rodríguez, Naturally-occurring iron minerals as inexpensive catalysts for CWPO, Appl Catal B 203 (2017) 166–173, <https://doi.org/10.1016/J.APCATB.2016.10.015>.
- [90] R.S. Ribeiro, A.M.T. Silva, J.L. Figueiredo, J.L. Faria, H.T. Gomes, Catalytic wet peroxide oxidation: a route towards the application of hybrid magnetic carbon

- nanocomposites for the degradation of organic pollutants. A review, *Appl Catal B*. 187 (2016) 428–460, <https://doi.org/10.1016/J.APCATB.2016.01.033>.
- [91] E. Serra-Pérez, C. Ferronato, A. Giroir-Fendler, S. Álvarez-Torrellas, G. Ovejero, J. García, Highly efficient Ru supported on carbon nanosphere nanoparticles for ciprofloxacin removal: Effects of operating parameters, degradation pathways, and kinetic study, *Ind. Eng. Chem. Res.* 59 (2020) 15515–15530.
- [92] Z. Fang, Z. Zhou, G. Xue, Y. Yu, Q. Wang, B. Cheng, Y. Ge, Y. Qian, Application of sludge biochar combined with peroxydisulfate to degrade fluoroquinolones: Efficiency, mechanisms and implication for ISCO, *J. Hazard. Mater.* 426 (2022), 128081, <https://doi.org/10.1016/J.JHAZMAT.2021.128081>.
- [93] Y. Zhao, H. Wang, J. Ji, X. Li, X. Yuan, L. Jiang, J. Yang, Y. Shao, X. Guan, Degradation of ciprofloxacin by peroxymonosulfate activation using catalyst derived from spent lithium-ion batteries, *J. Clean. Prod.* 362 (2022), 132442, <https://doi.org/10.1016/J.JCLEPRO.2022.132442>.